tion. The amount of recombinant α-galactosidase secreted from the HPY21G strain, a *S. cerevisiae* mutant harboring a human α-galactosidase cDNA, into the culture medium was approximately 290 μg per 1 l culture. The recovery of the enzyme through the purification procedure was 30%. Before treatment with α-mannosidase the purified enzyme was detected as a single band on SDS-PAGE, and its apparent molecular mass was determined to be 51 kDa on MALDI/TOF-MS. The molecular mass changed to 46 kDa following α-mannosidase digestion. The HPLC profile on a reversed-phase column contained a single peak. However, the *N*-terminal amino acid sequence could not be determined, indicating that some modification occurred at the *N*-terminus of yr-haGal. The specific enzyme activity of yr-haGal was 2.0 mmol h^{-1} mg $protein^{-1}$, which was a little higher than that purified by the previously described method (1.7 mmol h^{-1} mg $protein^{-1}$).

Monosaccharide composition of yr-haGal

The monosaccharide composition of the recombinant α-galactosidase was determined, and then compared with those of agalsidase alfa and agalsidase beta, which have been reported elsewhere (Lee et al. 2003). The results are shown in Table 1. The recombinant α-galactosidase produced in yeast has high-mannose-type sugar chains and contains no fucose or galactose residues. The content of M6P residues is 3.8 mol/mol protein, this value being a little higher than those of agalsidase alfa (1.8 mol/mol protein) and agalsidase beta (3.1 mol/mol protein).

Effect of yr-haGal on cultured human Fabry fibroblasts

Fabry fibroblasts were cultured in culture medium containing the indicated concentrations of the recombinant α-galactosidase for 18 h. Uptake of the enzyme by the Fabry fibroblasts was then investigated. The results are shown in Fig. 1. The α-galactosidase activity in untreated Fabry fibroblasts was almost nil, but it increased in response to addition of recombinant α-galactosidase dose-dependently, reaching a normal level when the recombinant α-galactosidase was added to the culture medium at a concentration of 0.25–1.0 μg/ml. Uptake of yr-haGal was decreased to 15% of the control level by the addition of 5 mM M6P, suggesting that incorporation of the enzyme depends largely on the M6P receptor.

We also investigated incorporation of the recombinant α-galactosidase protein into cultured Fabry fibroblasts, and its effect on cleavage of accumulated CTH by means of double staining for α-galactosidase and CTH. At first, double staining for CTH and LAMP-1, a lysosomal marker, was performed, which revealed that the accumulated CTH was localized in lysosomes of untreated Fabry cells (data not shown). The results of time-course analysis are shown in Fig. 2a. The recombinant α-galactosidase was added to the culture medium at a concentration of 3.0 μg/ml. After a 1-day incubation, immunofluorescence of α-galactosidase was detected and that of CTH was apparently decreased. After 3 days of culture, the maximum immunofluorescence for α-galactosidase was observed and the accumulated CTH was completely degraded. Thereafter, the immunofluorescence of α-galactosidase gradually decreased, but the disappearance of deposited CTH was maintained for at least 7 days. Next, we added recombinant α-galactosidase to the culture medium of Fabry fibroblasts at various concentrations from 0.5 to 3.0 μg/ml, and then cultured the cells for 3 days. Double staining for α-galactosidase and CTH revealed that clearance of the accumulated CTH in response to incorporation of the enzyme occurred dose-dependently (Fig. 2b).

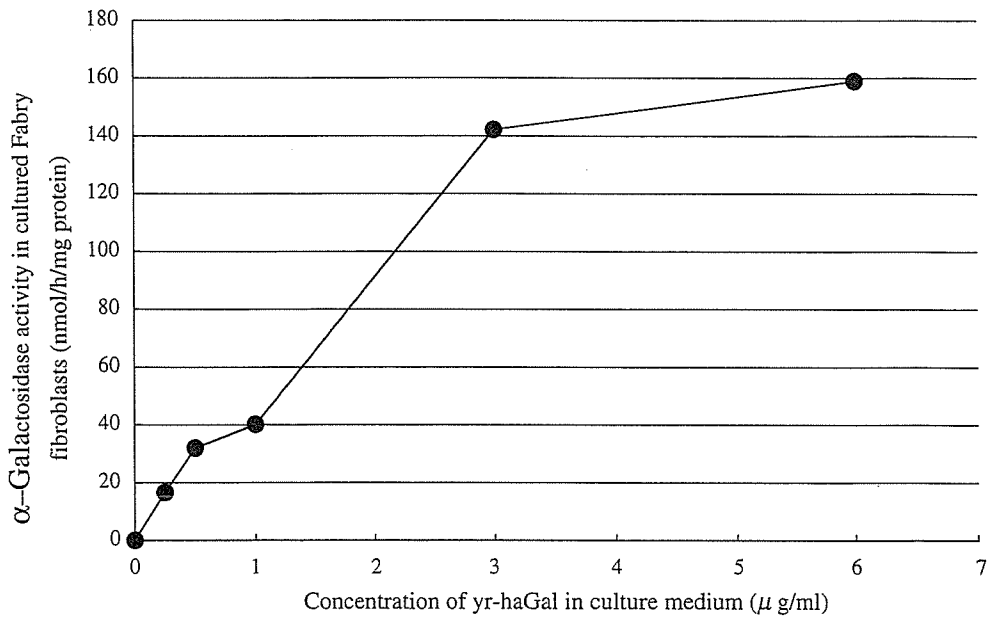

Fig. 1 Uptake by Fabry fibroblasts of the recombinant α-galactosidase produced in yeast cells (yr-haGal). Fabry fibroblasts were cultured in culture medium containing yr-haGal at concentrations of 0, 0.25, 0.5, 1.0, 3.0 and 6.0 μg/ml. After 18 h incubation, α-galactosidase activity in the cells was measured. The original α-galactosidase activity in Fabry fibroblasts was < 1 nmol h^{-1} mg $protein^{-1}$, and the normal range was 15–35 nmol h^{-1} mg $protein^{-1}$

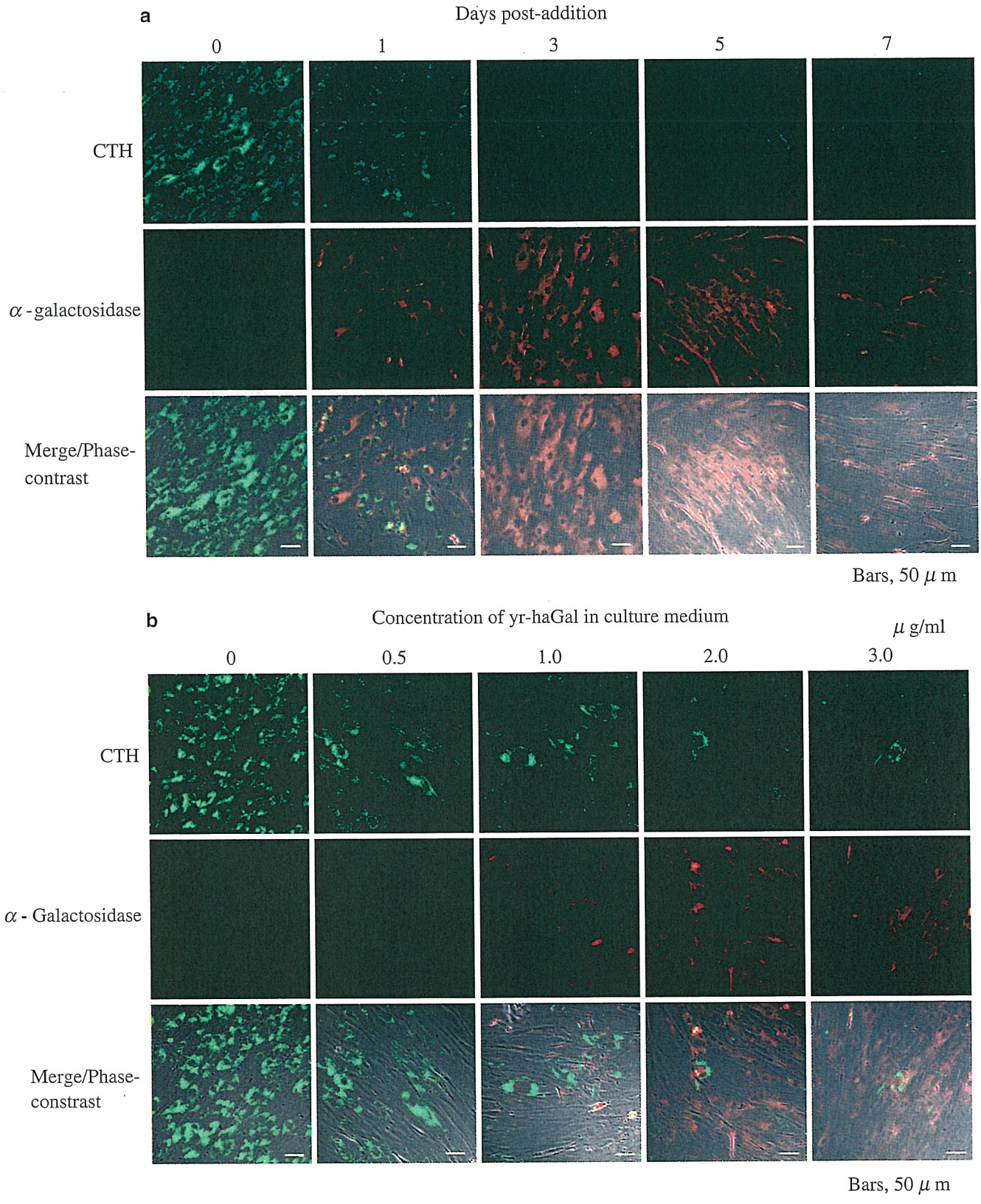

Fig. 2a,b Immunostaining for CTH and α-galactosidase in Fabry fibroblasts after addition of the recombinant α-galactosidase produced in yeast cells (*yr-haGal*). CTH, stained with an anti-CTH antibody (*green*); α-galactosidase, stained with anti-α-galactosidase antibodies (*red*); *Merge/Phase-contrast* overlapping images with these two fluorescent probes and phase-contrast images. Time-course (**a**) and dose-dependency (**b**). *Bars* 50μm

Effect of yr-haGal on Fabry mice

We injected recombinant α-galactosidase into Fabry mice to examine its therapeutic effect. We used agalsidase beta as a control enzyme because it has been reported that agalsidase beta is incorporated into affected organs in Fabry mice more than agalsidase alfa (Lee et al. 2003). As the specific enzyme activity in the yr-haGal we used (2.0 mmol h^{-1} mg $protein^{-1}$) was a little lower than that of the agalsidase beta sample (3.2 mmol h^{-1} mg $protein^{-1}$), we injected almost the same activity of the enzyme preparations into litter-matched Fabry mice for comparison.

After a single dose, 3.0 mg/kg body weight, of yr-haGal had been injected, its pharmacokinetics and biodistribution were examined and compared with those of agalsidase beta. The enzyme activity in plasma quickly increased, reaching a maximum level at 3 min after injection and then gradually decreasing. The pattern of the pharmacokinetics was essentially the same as that of agalsidase beta (Fig. 3). The biodistribution of yr-haGal and agalsidase beta after administration of a single dose is shown in Table 2. An apparent increase in α-galactosidase activity was observed in the organs of Fabry mice following yr-haGal administration. The degree of the enzyme activity increase in the kidneys and heart was almost the same as in the case of agalsidase beta, although that in the liver and spleen was a little lower than with agalsidase beta. The effect of yr-haGal on the degradation of tissue CTH was examined after repeated administration of the enzyme at 3.0 mg/kg body weight every week for four doses, followed by killing of the mice 6 days after the last injection. Immunohistochemical analysis revealed that the CTH deposited in the liver was cleaved (Fig. 4a). In kidney tissues, CTH immunofluorescence in the renal tubular cells was apparently decreased. Cleavage of the accumulated CTH in the glomeruli was insufficient although immunofluorescence was slightly decreased (Fig. 4b). In the heart, immunofluorescence of CTH accumulated in the tissue was apparently decreased after repeated injection of yr-haGal (Fig. 4c), as was also the case in the spleen (data not shown). In the dorsal root ganglia, no apparent degradation of accumulated CTH was observed (Fig. 4d). These findings were essentially the same as those found following administration of agalsidase beta. The results of quantitative analysis of CTH are shown in Table 3. Repeated administration of yr-haGal decreased the accumulated CTH in the liver to the level found in wild type mice, and decreased it to 70 and 30% of the levels in untreated Fabry mice in the kidneys and heart, respectively. The degree of degradation of CTH deposited in these tissues was almost the same as in the case of agalsidase beta. The decrease in accumulated CTH in the spleen upon administration of yr-haGal (to 30% of the untreated Fabry mice level) was smaller than that seen upon administration of agalsidase beta (to 10% of the untreated Fabry mice level). Morphological analysis revealed that many lamellar inclusion bodies, exhibiting accumulation of CTH, were present in the renal tubular cells of untreated Fabry mice (Fig. 5a), and that their number was markedly decreased after repeated administration of yr-haGal (Fig. 5b).

Immunoreactivity

The antigenicity of yr-haGal and agalsidase beta was examined by analyzing the cross-reactivity of antisera

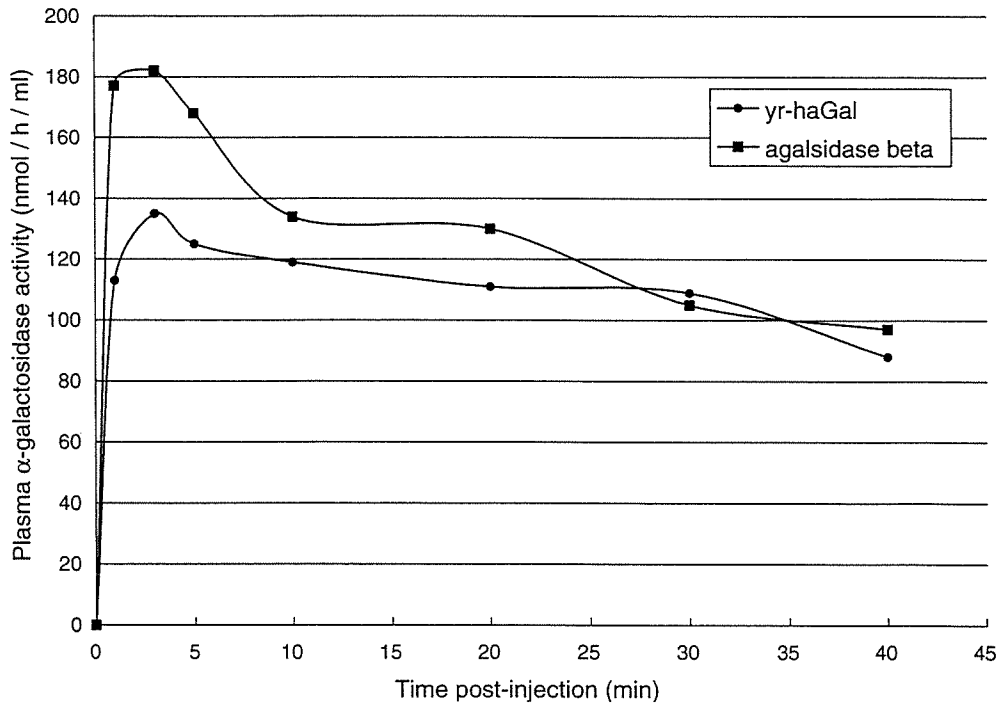

Fig. 3 Pharmacokinetics of yr-haGal and agalsidase beta. A single dose of yr-haGal or agalsidase beta was injected into Fabry mice; blood samples were collected and time courses of changes in plasma α-galactosidase activity were determined. Each value represents the mean from two mice

Table 2 α-Galactosidase activities (nmol h^{-1} mg $protein^{-1}$) in organs from Fabry mice treated with a single dose of yr-haGal or agalsidase beta. Fabry mice were injected with a single dose (almost the same enzyme activity) of yr-haGal (3 mg/kg body weight) or agalsidase beta (2 mg/kg body weight), and then were sacrificed 1 h after the administration. *Wild type* Wild type mice, *Fabry* untreated Fabry mice, *yr-haGal* Fabry mice treated with yr-haGal, *agalsidase beta* Fabry mice treated with agalsidase beta. Values are expressed as the means for two mice

	Liver	Kidney	Heart	Spleen
Wild type	30	11	7	29
Fabry	1	1	1	1
yr-haGal	57	52	90	42
agalsidase beta	174	87	76	100

derived from Fabry mice repeatedly injected with these preparations. The results are shown in Fig. 6. No significant antibodies unique to either enzyme preparation were found under the experimental conditions used.

Discussion

Production of recombinant human α-galactosidases in yeast cells has considerable advantages over production in mammalian cells, i.e., culture is easy, economical, and does not require fetal calf serum. Here, we used as a host a *S. cerevisiae* mutant in which two genes involved in *N*-linked mannan biosynthesis, *OCH1* and *MNN1*, are disrupted. The glycoprotein expressed in this cell line has mammalian-like *N*-linked high-mannose-type sugar chains and has no β-linked mannoside residues that are antigenic in humans (Chiba et al. 1998, 2002). As previously reported, treatment of the recombinant α-galactosidase expressed in this cell line with a bacterial α-mannosidase results in the exposure of M6P residues at the non-reducing ends of sugar chains (Chiba et al. 2002). As M6P residues are essential for incorporation of α-galactosidase into human cells via M6P receptors on the cell membrane (Kornfeld and Sly 2001), an α-galactosidase having many M6P residues would be beneficial for enzyme replacement therapy for Fabry disease. The yeast cell line also has a mutation in the *MNN4* gene, which regulates mannosylphosphorylation (Odani et al. 1996), resulting in the production of recombinant α-galactosidase with highly phosphorylated sugar chains. Productivity of the recombinant enzyme could be further improved in the future by careful choice of a host cell strain. We have preliminarily prepared a methylotrophic yeast cell line secreting recombinant α-galactosidase into the culture medium at a concentration of 12 mg/l, and attempts to obtain abundant enzyme protein using the improved purification method described in this report are underway.

The recombinant α-galactosidase added to the culture medium of Fabry fibroblasts was well incorporated into the cells. The accumulated CTH was cleaved, and the disappearance of deposited CTH held for at least 7 days. Incorporation of the enzyme was strongly inhibited in the presence of M6P. This finding allowed us to examine the effect of the recombinant α-galactosidase on Fabry mice.

Lee et al. (2003) reported that agalsidase beta has a higher percentage of phosphorylated oligomannose chains than agalsidase alfa, which results in improved binding of agalsidase beta to M6P receptors, and higher enzyme levels in the kidneys and heart, which are the organs most affected in Fabry disease, when tested at the same dose. Considering these results, we injected agalsidase beta into Fabry mice as a control in the experiment on the incorporation of yr-haGal into organs of Fabry mice, and its CTH-degrading activity. yr-haGal was successfully incorporated into the liver, kidneys, heart and spleen, and the CTH deposited in these organs was cleaved as in the case of agalsidase beta. However, degradation by these recombinant enzymes of CTH accumulated in the glomeruli was insufficient, although that in renal tubular cells was almost complete. Clinical trials using agalsidase beta have revealed that clearance of the CTH accumulated in podocytes was more limited than that observed in other cell types in kidney tissues (Thurnberg et al. 2002), suggesting that uptake of the recombinant α-galactosidases by podocytes is very low. There was a difference between yr-haGal and agalsidase beta in the degree of enzyme activity increase in the liver and spleen. This is probably due to differences in their sugar chain compositions. Asialylated complex-type oligosaccharides are involved in the uptake of lysosomal enzymes by hepatocytes in the liver via asialoglycoprotein receptors (Rosenfeld et al. 1986). Unlike agalsidase beta, the recombinant α-galactosidase produced in yeast cells does not have any complex-type sugar chains. Why agalsidase beta was incorporated into the spleen more than yr-haGal remains obscure. However, as Fabry disease does not affect the liver or spleen, the relatively low uptake of yr-haGal is thought not to be disadvantageous for enzyme replacement therapy for Fabry disease. Immunohistochemical analysis revealed that administration of either enzyme did not reduce granular immunofluorescence in the dorsal root ganglia from Fabry mice. Recently, we found that recombinant human β-hexosaminidases A and B, which are the lysosomal enzymes responsible for Sandhoff disease, produced in CHO cells, could be incorporated into cultured Schwann cells derived from dorsal root ganglia and adjacent peripheral nerves from Sandhoff mice via M6P receptors, but incorporation was apparently lower than that in the case of cultured Sandhoff fibroblasts

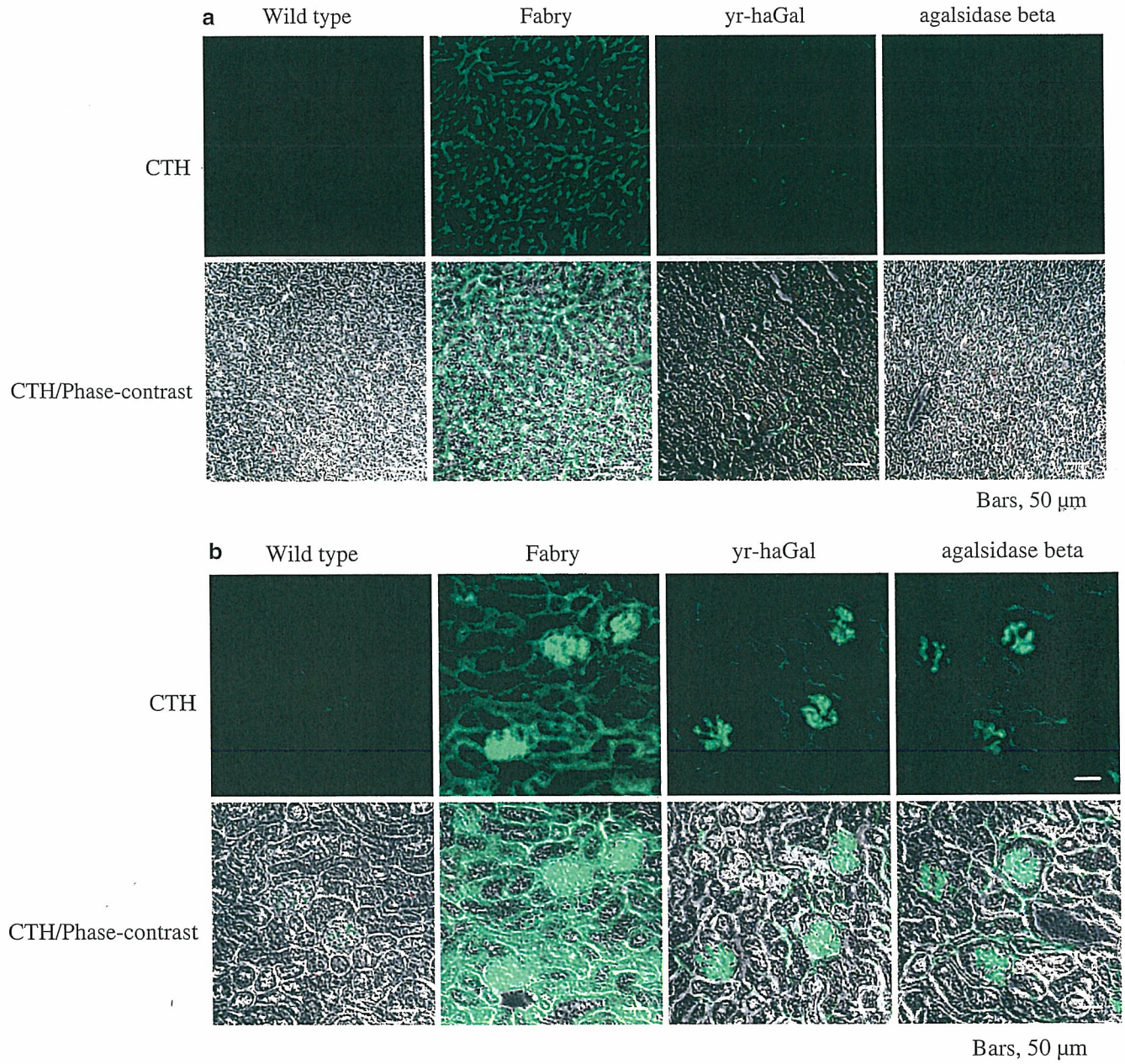

Fig. 4 Immunohistochemical analyses of the accumulated CTH in organs of Fabry mice, and its degradation by yr-haGal and agalsidase beta. Fabry mice were repeatedly injected with yr-haGal and agalsidase beta separately, and then immunostaining for CTH was performed. *CTH* Stained with an anti-CTH antibody (*green*), *CTH/Phase-contrast* overlapping CTH and phase-contrast images, *Phase-contrast* phase-contrast images. *Wild type* A wild type mouse, *Fabry* an untreated Fabry mouse, *yr-haGal* a Fabry mouse treated with yr-haGal, *agalsidase beta* a Fabry mouse treated with agalsidase beta. **a** Liver, **b** kidneys, **c** heart, **d** dorsal root ganglia. *Bars* 50 μm

(Ohsawa et al. 2005). The total number of M6P receptors on the surface of neural cells might be less than that on non-neural cells. Intravascularly administered lysosomal enzymes are barely incorporated into neural cells. Phase 3 clinical trials for agalsidase beta revealed that there were no significant differences in improvement of pain in the peripheral extremities between a group of patients treated with agalsidase beta and the placebo group (Eng et al. 2001). Some improvement is required for targeting of the enzyme to neural cells, i.e., the production of a recombinant α-galactosidase with abundant M6P residues.

It is known that the administration of agalsidase alfa and agalsidase beta frequently causes infusion reactions, mainly allergic reactions (Schiffmann et al. 2000; Eng et al. 2001). Thus, we examined the levels of antibodies against yr-haGal in sera of recurrently injected Fabry mice by means of ELISA, but no specific antibodies for yr-haGal were detected, as was also the case of agalsidase beta under the experimental conditions used.

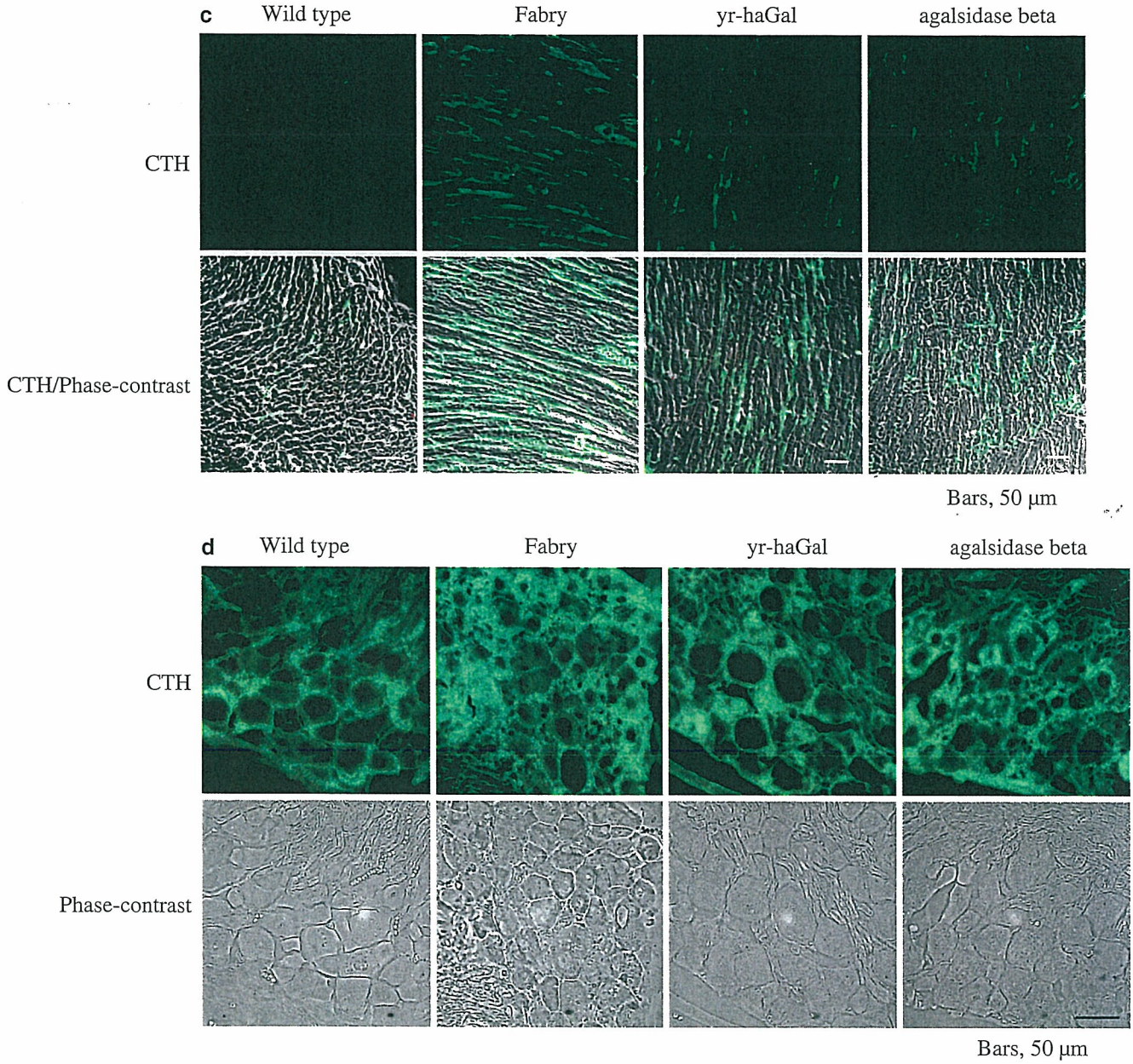

Fig. 4 (Contd.)

Table 3 Ceramide trihexoside (CTH) levels (nmol/mg protein) in organs from Fabry mice treated with four doses of yr-haGal or agalsidase beta. Fabry mice were injected with almost the same enzyme activity of yr-haGal (3 mg/kg body weight) or agalsidase beta (2 mg/kg body weight) separately every week for four doses, and were sacrificed 6 days after the last injection. *Wild type* Wild type mice, *Fabry* untreated Fabry mice, *yr-haGal* Fabry mice treated with yr-haGal, *agalsidase beta* Fabry mice treated with agalsidase beta. Values are expressed as means ±SEM ($n=3$)

	Liver	Kidney	Heart	Spleen
Wild type	0.07±0.01	0.78±0.10	0.00±0.00	0.34±0.11
Fabry	1.40±0.41	5.36±0.08	2.01±0.21	3.05±0.33
yr-haGal	0.03±0.02	3.89±0.36	0.58±0.16	0.96±0.41
agalsidase beta	0.09±0.06	3.39±0.14	0.67±0.34	0.37±0.06

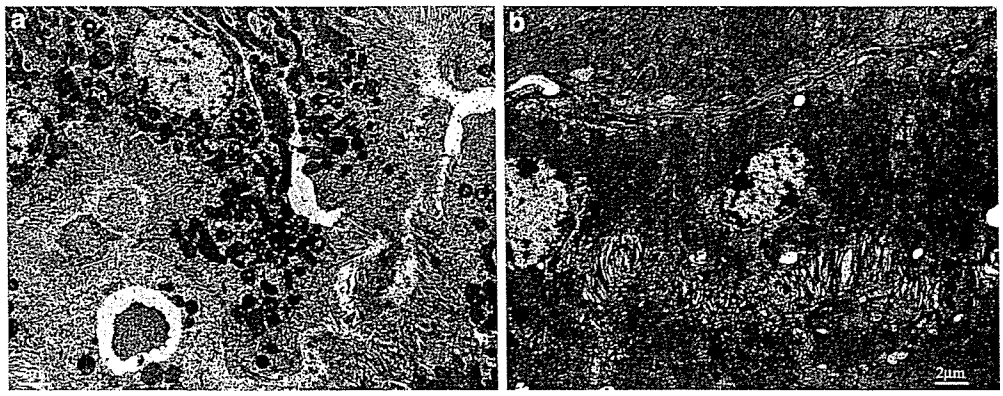

Fig. 5a,b Morphological effects of repeated administration of yr-haGal on renal tubular cells of Fabry mice. yr-haGal was repeatedly injected into Fabry mice; kidney tissues were then examined by electron microscopy. **a** An untreated Fabry mouse. **b** A Fabry mouse treated with yr-haGal. Many lamellar inclusion bodies can be seen in the renal tubular cells of the untreated Fabry mice, and the number of lamellar inclusion bodies is apparently decreased after repeated administration of yr-haGal. *Bar* 2 μm

In conclusion, we produced in yeast cells a recombinant α-galactosidase with M6P residues at the non-reducing ends of *N*-linked sugar chains. This recombinant enzyme was incorporated into the liver, kidneys, heart and spleen, and degraded the accumulated CTH in these tissues, although cleavage of the CTH accumulated in the dorsal root ganglia was insufficient. As production of recombinant α-galactosidase in yeast is easy and economical, and does not require fetal calf serum, yr-haGal is highly promising as an enzyme source for enzyme replacement therapy for Fabry disease.

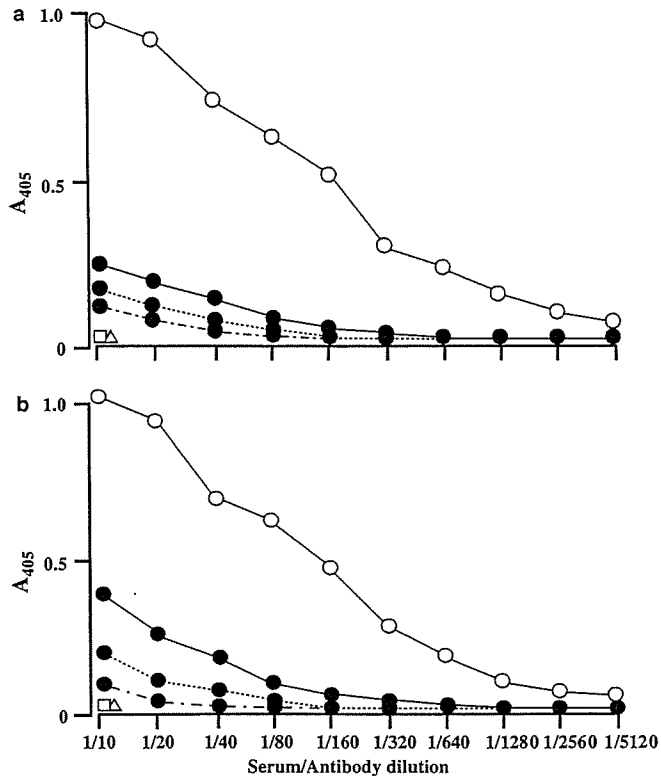

Fig. 6 Antigenicity of yr-haGal and agalsidase beta. ELISA was performed to determine whether Fabry mice recurrently injected with yr-haGal (**a**) or agalsidase beta (**b**) produced antibodies to the enzymes or not. *Open circles* Rabbit anti-α-galactosidase antibodies, *closed circles* Fabry mouse sera treated with the enzymes (yr-haGal and agalsidase beta), *open squares* serum from an untreated Fabry mouse, *open triangles* serum from an untreated wild type mouse

Acknowledgements We wish to thank Drs. Ashok B. Kulkarni (Gene Targeting Facility and Functional Genomics Unit, NIDCR, NIH) and Toshio Ohshima (Laboratory for Developmental Neurology, Brain Science Institute, RIKEN), and also Drs. Ryoichi Kase, Fumiko Matsuzawa and Sei-ichi Aikawa (The Tokyo Metropolitan Institute of Medical Science) for their technical support. This work was partly supported by grants from the Tokyo Metropolitan Government, the Japan Society for the Promotion of Science, the Ministry of Education, Science, Sports and Culture, and the Ministry of Health, Labor and Welfare of Japan.

References

Chiba Y, Suzuki M, Yoshida S, Yoshida A, Ikenaga H, Takeuchi M, Jigami Y, Ichishima E (1998) Production of human compatible high mannose-type ($Man_5GlcNAc_2$) sugar chains in *Saccharomyces cerevisiae*. J Biol Chem 273:26298-26304

Chiba Y, Sakuraba H, Kotani M, Kase R, Kobayashi K, Takeuchi M, Ogasawara S, Maruyama Y, Nakajima T, Takaoka Y, Jigami Y (2002) Production in yeast of α-galactosidase A, a lysosomal enzyme applicable to enzyme replacement therapy for Fabry disease. Glycobiology 12:821–828

Desnick RJ, Ioannou YA, Eng CM (2001) α-Galactosidase A deficiency: Fabry disease. In: Scriver CR, Beaudet AL, Sly WS, Valle D (eds) The metabolic and molecular bases of inherited disease, 8th edn. McGraw-Hill, New York, pp 3733–3774

Desnick RJ, Brady RO, Barranger J, Collins AJ, Germain DP, Goldman M, Grabowski G, Packman S, Wilcox WR (2003) Fabry disease, an under-recognized multisystemic disorder: expert recomendations for diagnosis, management, and enzyme replacement therapy. Ann Intern Med 138:338–346

Eng CM, Banikzzemi M, Gordon RE, Goldman M, Phelps R, Kim L, Gass A, Winston J, Dikman S, Fallon JT, Brodie S, Stacy CB, Mehta D, Parsons R, Norton K, O'Callaghan M, Desnick RJ (2001a) A phase 1/2 clinical trial of enzyme replacement in Fabry disease: pharmacokinetic, substrate clearance, and safety studies. Am J Hum Genet 68:711–722

Eng CM, Guffon N, Wilcox WR, Germain DP, Lee P, Waldek S, Caplan L, Linthorst GE, Desnick RJ (2001b) Safety and efficacy of recombinant human α-galactosidase A replacement therapy in Fabry's disease. N Engl J Med 345:9–16

Fukushima M, Tsuchiyama Y, Nakato T, Yokoi T, Ikeda H, Yoshida S, Kusumoto T, Itoh K, Sakuraba H (1995) A female heterozygous patient with Fabry's disease with renal accumulation of trihexosylceramide detected with a monoclonal antibody. Am J Kidney Dis 26:952–955

Ishii S, Kase R, Sakuraba H, Fujita S, Sugimoto M, Tomita K, Semba T, Suzuki Y (1994) Human α-galactosidase gene expression: significance of two peptide regions encoded by exons 1–2 and 6. Biochim Biophys Acta 1204:265–270

Itoh K, Kotani M, Tai T, Suzuki H, Utsunomiya T, Inoue H, Yamada H, Sakuraba H, Suzuki Y (1993) Immunoflorescence imaging diagnosis of Fabry heterozygotes using confocal laser scanning microscopy. Clin Genet 44:302–306

Itoh K, Takenaka T, Nakao S, Setoguchi M, Tanaka H, Suzuki T, Sakuraba H (1996) Immunofluorescence analysis of globotriaosylceramide accumulated in the hearts of variant hemizygotes and heterozygotes with Fabry disease. Am J Cardiol 78:116–117

Kornfeld S, Sly WS (2001) I-cell disease and pseudo-Hurler polydystrophy: disorders of lysosomal enzyme phosphorylation and localization. In: Scriver CR, Beaudet AL, Sly WS, Valle D (eds) The metabolic and molecular bases of inherited disease, 8th edn. McGraw-Hill, New York, pp 3469–3482

Kotani M, Kawashima I, Ozawa H, Ogura K, Ariga T, Tai T (1994) Generation of one set of murine monoclonal antibodies specific for globo-series glycolipids: evidence for differential distribution of the glycolipids in rat small intestine. Arch Biochem Biophys 310:89–96

Kotani M, Yamada H, Sakuraba H (2004) Cytochemical and biochemical detection of intracellularly accumulated sialyl glycoconjugates in sialidosis and galactosialidosis fibroblasts with *Maakia amurensis*. Clin Chim Acta 344:131–135

Lee K, Jin X, Zhang K, Copertino L, Andrews L, Baker-Malcolm J, Geagen L, Qui H, Seiger K, Barngrover D, McPherson JM, Edmunds T (2003) A biochemical and pharmacological comparison of enzyme replacement therapies for the glycolipid storage disorder Fabry disease. Glycobiology 13:305–313

Lyon MF (1962) Sex chromatin and gene action in the mammalian X-chromosome. Am J Hum Genet 14:135–148

Mehta A, Ricci R, Widmer U, Dehout F, Garcia de Lorenzo A, Kampmann C, Linhart A, Sunder-Plassmann G, Ries M, Beck M (2004) Fabry disease defined: baseline clinical manifestations of 366 patients in the Fabry Outcome Survey. Eur J Clin Invest 34:236–242

Mayes JS, Scheerer JB, Sifers RN, Donaldson ML (1981) Differential assay for lysosomal α-galactosidase in human tissues and its application to Fabry's disease. Clin Chim Acta 112:247–251

Nakao S, Takenaka T, Maeda. M, Kodama C, Tanaka A, Tahara M, Yoshida A, Kuriyama M, Hayashibe H, Sakuraba H, Tanaka H (1995) An atypical variant of Fabry's disease in men with left ventricular hypertrophy. N Engl J Med 333:288–293

Odani T, Shimma Y, Tanaka A, Jigami Y (1996) Cloning and analysis of the *MNN4* gene required for phosphorylation of *N*-linked oligosaccharides in *Saccharomyces cerevisae*. Glycobiology 6:805–810

Ohsawa M, Kotani M, Tajima Y, Tsuji D, Ishibashi Y, Kuroki A, Itoh K, Watabe K, Sango K, Yamanaka S, Sakuraba H (2005) Establishment of immortalized Schwann cells from Sandhoff mice and corrective effect of recombinant human β-hexosaminidase A on the accumulated GM2 ganglioside. J Hum Genet 50:460–467

Rosenfeld EL, Belenky DM, Bystrov NK (1986) Interaction of hepatic asialoglycoprotein receptor with asialoorosomucoid and galactolyzed lysosomal α-glucosidase. Biochim Biophys Acta 883:306–312

Sakuraba H, Yanagawa Y, Igarashi T, Suzuki Y, Suzuki T, Watanabe K, Ieki K, Shimoda K, Yamanaka T (1986) Cardiovascular manifestations in Fabry's disease. A high incidence of mitral valve prolapse in hemizygotes and heterozygote. Clin Genet 29:276–283

Sakuraba H, Oshima A, Fukuhara Y, Shimmoto M, Nagao Y, Bishop DF, Desnick RJ, Suzuki Y (1990) Identification of point mutations in the α-galactosidase A gene in classical and atypical hemizygotes with Fabry disease. Am J Hum Genet 47:784–789

Schiffmann R, Murray GJ, Treco D, Daniel P, Sellos-Moura M, Myers M, Quirk JM, Zirzow GC, Borowski M, Loveday K, Anderson T, Gillespie F, Cliver KL, Jeffries NO, Doo E, Liang TJ, Kreps C, Gunter K, Frei K, Crutchfield K, Selden RF, Brady RO (2000) Infusion of α-galactosidase A reduces tissue globotriaosylceramide storage in patients with Fabry disease. Proc Natl Acad Sci USA 97:365–370

Takahashi H, Hirai Y, Migita M, Seino Y, Fukuda Y, Sakuraba H, Kase R, Kobayashi T, Hashimoto Y, Shimada T (2002) Long-term systemic therapy of Fabry disease in a knockout mouse by adeno-associated virus-mediated muscle-directed gene transfer. Proc Natl Acad Sci USA 99:13777–13782

Takashiba M, Chiba Y, Arai E, Jigami Y (2004) Analysis of mannose-6-phosphate labeled with 8-aminopyrene-1,3,6-trisulfonate by capillary electrophoresis. Anal Biochem 332:196–198

Thurnberg BL, Rennke H, Colvin RB, Dikman S, Gordon RE, Collins AB, Desnick RJ, O'Callaghan M (2002) Globotriaosylceramide accumulation in the Fabry kidney is cleared from multiple cell types after enzyme replacement therapy. Kidney Int 62:1933–1946

Sox10 regulates ciliary neurotrophic factor gene expression in Schwann cells

Yasuhiro Ito*, Stefan Wiese*, Natalja Funk*, Alexandra Chittka*, Wilfried Rossoll*, Heike Bömmel*, Kazuhiko Watabe†, Michael Wegner‡, and Michael Sendtner*§

*Institute for Clinical Neurobiology, University of Wuerzburg, D-97080 Wuerzburg, Germany; †Department of Molecular Neuropathology, Tokyo Metropolitan Institute for Neuroscience, 2-6 Musashidai, Fuchu-shi, Tokyo 183-8526, Japan; and ‡Institute of Biochemistry, Erlangen University, D-91054 Erlangen, Germany

Communicated by Hans Thoenen, Max Planck Institute of Neurobiology, Martinsried, Germany, March 29, 2006 (received for review November 16, 2005)

Ciliary neurotrophic factor (Cntf) plays an essential role in postnatal maintenance of spinal motoneurons. Whereas the expression of this neurotrophic factor is low during embryonic development, it is highly up-regulated after birth in myelinating Schwann cells of rodents. To characterize the underlying transcriptional mechanisms, we have analyzed and compared the effects of various glial transcription factors. In contrast to Pit-1, Oct-1, Unc-86 homology region (POU) domain class 3, transcription factor 1 (Oct6/SCIP/Tst-1) and paired box gene 3 (Pax3), SRY-box-containing gene 10 (Sox10) induces Cntf expression in Schwann cells. Subsequent promoter analysis using luciferase reporter gene and EMSA identified the corresponding response elements within the *Cntf* promoter. Overexpression of Sox10 in primary sciatic nerve Schwann cells leads to a >100-fold up-regulation of Cntf protein, and suppression of Sox10 by RNA interference in the spontaneously immortalized Schwann cell line 32 reduces Cntf expression by >80%. Mice with heterozygous inactivation of the *Sox10* gene show significantly reduced Cntf protein levels in sciatic nerves, indicating that Sox10 is necessary and sufficient for regulating Cntf expression in the peripheral nervous system.

promoter | Hirschsprung disease | Oct6 | neuropathy | Pax3

Schwann cells play an important role for maintenance of motoneurons. Their development is regulated by various transcription factors (1), including paired box gene 3 (Pax3) (2), Pit-1, Oct-1, Unc-86 homology region (POU) domain class 3, transcription factor 1 (Oct-6/SCIP/Tst-1) (3–6), and SRY-box-containing gene 10 (Sox10) (7, 8). *Ciliary neurotrophic factor* (*Cntf*) belongs to a family of neuropoietic cytokines that promote neuronal survival (9–13) and peripheral nerve regeneration (14–16). Targeted inactivation of the *Cntf* gene in mice revealed its role in postnatal maintenance of motoneurons (17, 18). Moreover, endogenous Cntf modulates onset and severity of disease in patients and mouse models for motoneuron disease and other neurological disorders (19–21). In progressive motor neuronopathy and wobbler mice, Cntf treatment protects motoneurons from cell death and improves motor performance (22, 23), indicating that this factor is a major mediator of the protective effects of Schwann cells, both under physiological and pathological conditions.

Myelinating Schwann cells in the peripheral nervous system are the richest source of Cntf in adult mammals (9, 10, 24). Expression of Cntf in the peripheral nervous system rises at the end of the first postnatal week. The control mechanisms that regulate and restrict *Cntf* expression to myelinating Schwann cells are still not known. To analyze the regulation of *Cntf* expression, we have cloned a 4.7-kb fragment containing the complete 5′ region of the murine Cntf gene up to the neighboring zinc finger protein (*Zfp*) gene. Using deletion and mutation analysis, we found that Cntf gene expression is controlled by several glial transcriptional factors. Sox10 was identified as a key regulator of Cntf expression. Sox10 overexpression in cultured primary Schwann cells leads to a >100-fold up-regulation of Cntf protein levels. In addition, Cntf levels are significantly lower in sciatic nerves of *Sox10*+/− mice, indicating that Sox10 acts as a major physiological regulator of Cntf gene expression *in vivo*.

Results

Reduced Cntf Expression in *Sox10*+/− Mice. In comparison to other Schwann cell-specific transcription factors, Sox10 expression is most closely linked to Cntf up-regulation during postnatal development (8). We therefore analyzed Cntf expression in *Sox10*+/− mutant mice (8). Mice with homozygous mutation of the *Sox10* gene already start to die around embryonic day 13.5 (25, 26). Sox10 expression increases from postnatal day (P)1 to P3, whereas a strong increase of Cntf expression was first detectable at P7 (Fig. 1*A*). Cntf protein levels are reduced by >50% (Fig. 1 *B* and *C*) in *Sox10*+/− mice.

To get more insight into the physiological relevance of this finding, we overexpressed Sox10 in primary Schwann cells from P4 rat sciatic nerves. This treatment resulted in a >100-fold induction of Cntf protein levels (Fig. 1 *D* and *E*). Thus, Sox10 appears sufficient for up-regulating Cntf expression in early postnatal Schwann cells. We then investigated the expression of Cntf in the spontaneously immortalized Schwann cell line 32 (IMS32) (27). In contrast to primary Schwann cells, this cell line expresses constitutively relatively high levels of Cntf (Fig. 1*G*) and therefore was used for this experiment. Suppression of Sox10 by RNA interference leads to significant reduction ($P < 0.001$) of Cntf expression (Fig. 1*F*).

Characterization of the Regulatory Elements and Transcription Initiation Sites Within the *Cntf* Promoter. To characterize the *Cntf* promoter region, we cloned a 6.5-kb DNA fragment containing the complete *Cntf* gene including the 4.7-kb 5′ flanking region up to *Zfp*, the neighboring gene (28). The stop codon of *Zfp* was located at −4,647 bp from the start codon of *Cntf*. We performed 3′ RACE to identify the poly(A) signal for *Zfp* and found a canonical AATAAA site located at −4,549 bp from the Cntf ATG start codon. Because the *Cntf* promoter sequence does not contain a TATA box (29), we carried out 5′ RACE. For human and rat Cntf, only one initiation site has been identified so far (29). We found three additional initiation sites (−10, −32, −68, and −74 bp from the ATG start codon) for mouse *Cntf* (see Fig. 5, which is published as supporting information on the PNAS web site). Five, four, six, and one clone of 16 analyzed were identified for these four transcription start sites, respectively. In addition, using sequence analysis, we identified several potential

Conflict of interest statement: No conflicts declared.

Abbreviations: Cntf, ciliary neurotrophic factor; IMS32, immortalized Schwann cell line 32; S1, S2, and S3, Sox10 high mobility group type DNA-binding motifs 1, 2, and 3; S1m, S2m, and S3m, mutated S1, S2, and S3; P*n*, postnatal day *n*.

§To whom correspondence should be addressed at: Institute for Clinical Neurobiology, Josef-Schneider-Strasse 11, University of Wuerzburg, D-97080 Wuerzburg, Germany. E-mail: sendtner@mail.uni-wuerzburg.de.

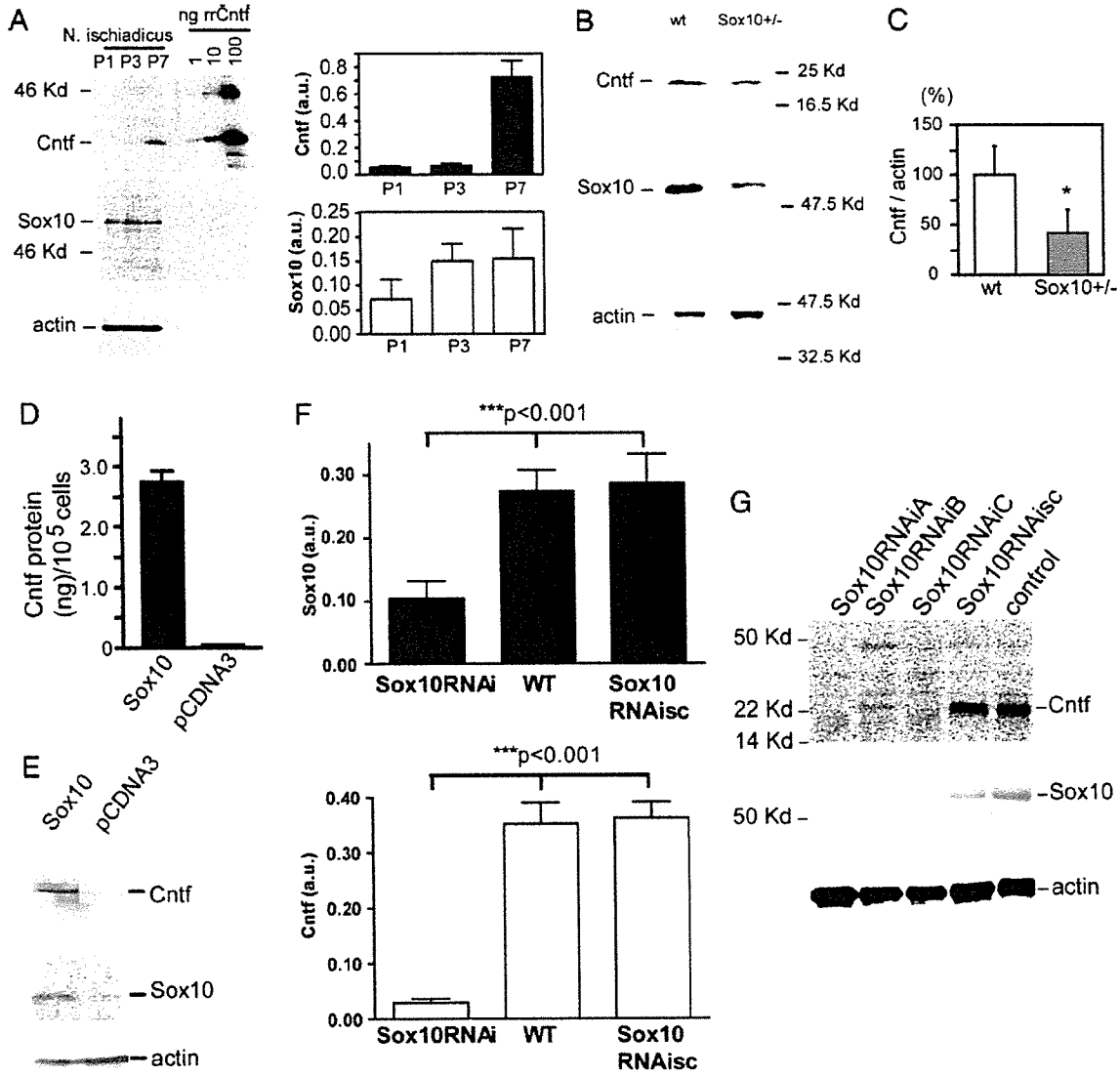

Fig. 1. Expression of Sox10 and Cntf in sciatic nerve of wild-type and *Sox10+/−* mutant mice. (*A Left*) Western blot analysis of sciatic nerve (*nervus ischiadicus*) extracts from P1, P3, and P7 wild-type mice. Western blots were probed for Sox10 and Cntf and reprobed against actin as a control for equal loading. rrCntf, recombinant rat Cntf. (*A Right*) Semiquantitative analysis of Cntf and Sox10 expression from three independent experiments. Error bars represent SD. (*B*) Western blot analysis of sciatic nerve extracts from adult wild-type and *Sox10+/−* mice. Cntf protein was detected as one band at 22 kDa. Sox10 protein content is reduced in sciatic nerve extract of *Sox10+/−* mice. (*C*) The density of the Cntf immunoreactive bands was measured in three independent blots. Signals were normalized against the actin signal and are shown as percentage of wild-type levels. Error bars represent SD. *, $P < 0.05$. (*D*) Cntf expression is elevated in primary Schwann cells after transient transfection of Sox10. Expression levels were estimated by measuring signal density from Western blots. A representative example is shown in *C*. Expression levels (mean ± SD) were quantified by using the AIDA software program. (*E*) Cntf expression in primary rat Schwann cells after transfection of Sox10. (*F*) Cntf expression is reduced after transfection of Sox10 RNA interference (RNAi) into the IMS32 Schwann cell line. Expression levels for Sox10 and Cntf were estimated by measuring signal density from Western blots. A representative example is shown in *G*. Expression levels (mean ± SD) were quantified by using the AIDA software program. (*G*) Cntf and Sox10 expression in native IMS32 cells and after transient transfection of Sox10RNAiA, Sox10RNAiB, or Sox10RNAiC (see also Table 1). Sox10RNAisc is a scrambled sequence RNA interference corresponding to Sox10RNAiA that was used as a specificity control.

binding sites for specific transcription factors including Pax3, Oct6/SCIP/Tst-1, and Sox proteins (see Figs. 5 and 6*A*, which are published as supporting information on the PNAS web site). Comparison of the human and mouse *Cntf* promoter regions revealed that the putative Sox10 binding sites are highly conserved (Fig. 6 *B* and *C*).

Analysis of the *Cntf* Promoter by Luciferase Reporter Assays. To characterize the role of the identified putative response elements for Pax3, Oct-6/SCIP/Tst-1, and Sox10 (see Figs. 5 and 6) in the *Cntf* promoter, various reporter gene constructs were established (see Fig. 7*A*, which is published as supporting information on the PNAS web site) and transfected into the Schwann cell line IMS32, the neuroblastoma cell line Neuro2A, and the green monkey simian virus 40-transfected kidney fibroblast cell line Cos7. We have included these different cell lines in our study to investigate the regulation of Cntf expression in a neural cell line (Neuro2A), in a Schwann cell line (IMS32), and in a cell line not derived from the nervous system (Cos7) as a control. The Schwann cell line IMS32 was used instead of primary Schwann

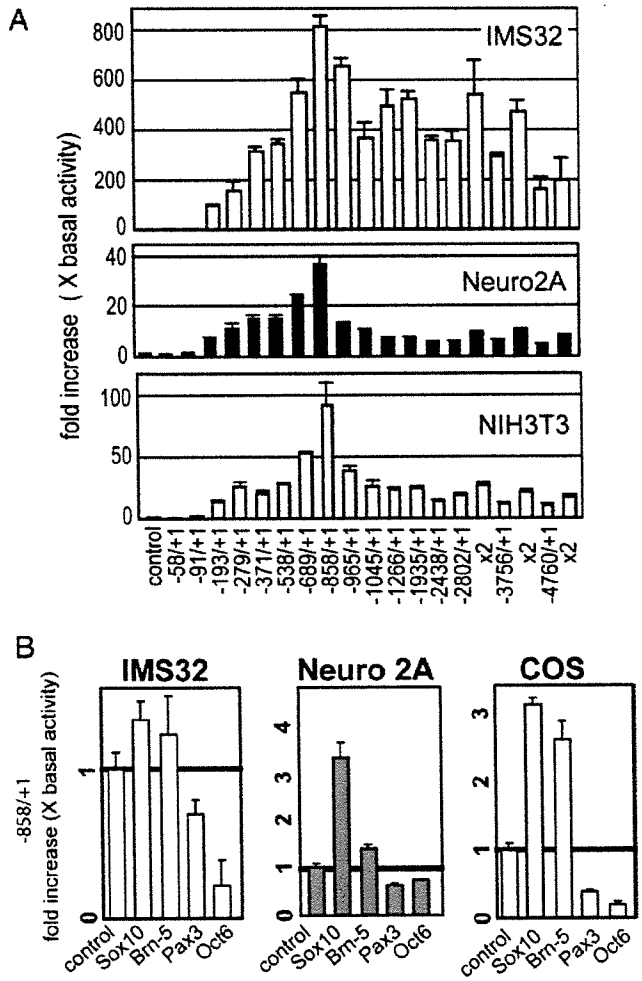

Fig. 2. Promoter constructs and analysis of reporter expression in various cell types. (*A*) Sixteen luciferase reporter constructs with different lengths of the *Cntf* promoter were generated for transient transfection in various cell lines (Fig. 7*A*). Transcriptional activity was determined after transfection into the Schwann cell line IMS32, Neuro2A, and NIH 3T3 cells. Relative activity was highest in IMS32 (up to 800× basal activity). The construct −858/+1 revealed highest activity in all cell lines. One microgram of the reporter plasmid was used for transient transfection. As a control, empty vector was transfected. For constructs longer than 2.5 kb (−2,802/+1, −3,856/+1, and −4,760/+1), double amounts of plasmid were transfected to adjust for reduced number of molecules. For each construct, at least three independent transfection experiments with at least three independent plates in each experiment were performed, and luciferase activities are shown as mean ± SD. As a control, empty vector was transfected. (*B*) Expression plasmids for Sox10, Brn-5, Oct-6, and Pax3 were transfected into Neuro2A, Cos7, and IMS32 cells. Data show promoter activity of the cotransfected −858/+1 reporter construct relative to control (pCDNA3) transfected cells. Similar data were obtained with the −4,760/+1 construct (data not shown).

cells because it was not possible to expand the primary Schwann cells at sufficient numbers for the promoter analyses. In all cell lines, the −858/+1 construct showed strongest expression of the reporter (Fig. 2*A*) and therefore was used for subsequent analyses. Stepwise induction of gene expression was found in three regions: from base pair −91 to base pair −193, from base pair −193 to base pair −371, and from base pair −538 to base pair −858 from the ATG codon (Fig. 2*A*). In contrast, the region between base pair −371 and base pair −538 did not contribute to increased reporter gene expression. Any construct longer than −858/+1 revealed no additive up-regulation. In Neuro2A and immortalized fibroblasts (NIH3T3), highly reduced reporter gene expression was observed with constructs including the base pair −858 to base pair −965 region. In IMS32 cells, strong reduction was recognized within a region from base pair −965 to base pair −1,045. This observation could indicate that regulatory elements for transcriptional repression exist distal to base pair −858. For further studies, the −4,760/+1 construct was also used because it contained the complete *Cntf* promoter including these putative repressor elements.

In the IMS32 Schwann cell line, basal levels for *Cntf* reporter gene activity were ≈27-fold higher than in Neuro2A cells and 20-fold higher than in Cos7 cells. We then transfected the −856/+1 reporter gene construct with expression plasmids for Pax3, Oct-6/SCIP/Tst-1, Sox10, and Pit-1, Oct-1, Unc-86 conserved region (POU) domain, class 6, transcription factor 1 (Brn5) (Fig. 2*B*). Cos7 cells do not express endogenous Pax3 (30), Oct-6/SCIP/Tst-1 (31), and Sox10 (32). Neuro2A cells do not express Pax3, Oct-6/SCIP/Tst-1, and Sox10 (2, 33). In both cell lines, transfection of Sox10 induced reporter gene expression ≈3-fold above baseline level (Fig. 2*B*). In IMS32 cells, Sox10, Pax3, Brn5, and Oct6/SCIP/Tst-1 are expressed endogenously (27, 34). This finding could explain why only a slight induction was observed after Sox10 or Brn5 transfection in IMS32 cells. Results were virtually identical with the −858/+1 construct and the −4,760/+1 promoter construct (data not shown). Brn5 led to enhanced promoter activity in Cos7 cells but not in Neuro2A or IMS32 cells. Highest induction was observed in Sox10-transfected cell lines, whereas Pax3 and Oct6 repressed *Cntf* reporter activity in all cell lines.

Identification of Sox10 Responsive Elements in the *Cntf* Promoter. We then performed reporter assays to further characterize Sox10-dependent activation. The Neuro2A cell line was used because it does not express Sox10 endogenously and thus could be used for cotransfection of truncated *Cntf* promoter-luciferase plasmids and Sox10-expression vectors (Fig. 3*A*). Sox10-dependent induction was found with constructs including regions between base pair −279 and base pair −328 and between base pair −538 and base pair −858 (Fig. 3*B*).

Sox10 is a high mobility group type DNA-binding protein. High mobility group proteins bind to a 7-bp consensus sequence (A/T)(A/T)CAA(A/T)G (33, 35). Such consensus elements are found at base pair positions −287 and −293 of the *Cntf* promoter, and two additional elements with one mismatch are localized at base pair −592 to base pair −600 and base pair −660 to base pair −666 (Fig. 5). We designated these sequences as "Sox10 high mobility group type DNA-binding motif" 1 (S1) (base pair −287 to base pair −293), S2 (base pair −592 to base pair −600), and S3 (base pair −660 to base pair −666), respectively. To evaluate the influence of Sox10 on these promoter sites, we produced mutant reporter gene constructs by replacing the consensus sequences with GCGC base pairs (see Table 1, which is published as supporting information on the PNAS web site). These mutant reporter constructs (Fig. 7*B*) were cotransfected with Sox10 expression plasmids into Neuro2A cells, and promoter activity was measured by luciferase assays (Fig. 3*C*). In comparison to the wild-type *Cntf* promoter construct, mutated S1 (S1m) showed a 56% reduction, S2m showed a modest reduction (28%), and S3 showed a weak reduction (17%). These results indicate that these putative Sox10 binding sites are important for Cntf expression but that their contributions are not equivalent. The S1 site appears most critical for Sox10-dependent induction. Combined mutation of all three putative Sox10 binding sites (S123m) resulted in a virtually complete loss of luciferase reporter gene induction by Sox10 (Fig. 3*C*).

We also performed EMSA to demonstrate direct binding of Sox10 to the S1, S2, and S3 sites. Nuclear extract from COS cells expressing Sox10 protein (Fig. 4*A*) showed shifted bands with a

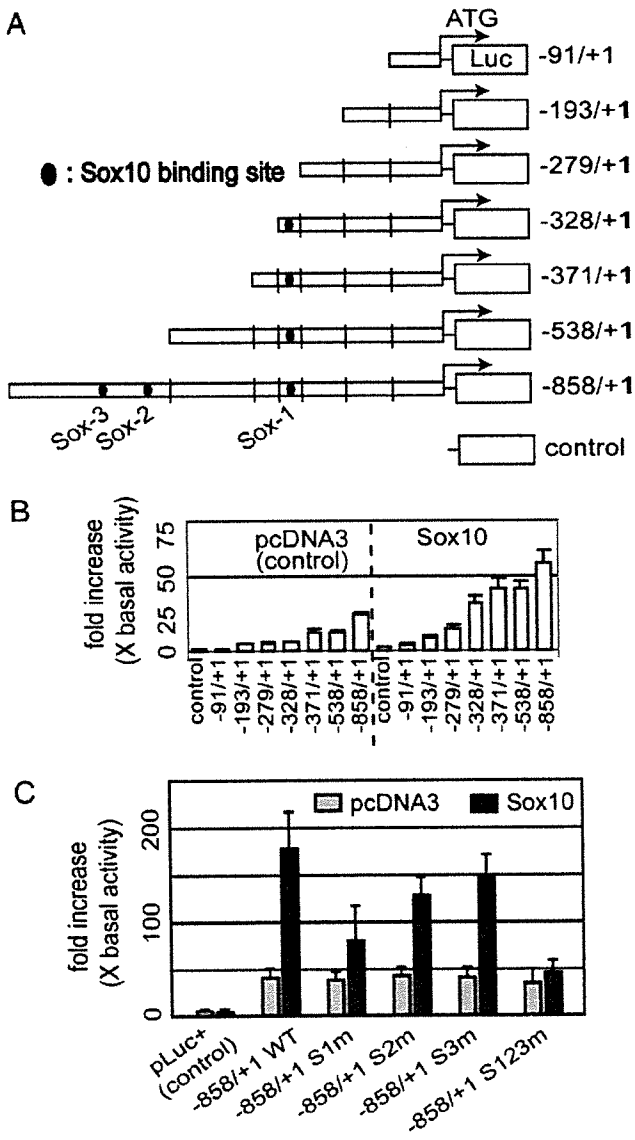

Fig. 3. Effect of Sox10 on *Cntf* promoter activity. (*A*) Cotransfection of Sox10 with *Cntf* promoter-luciferase constructs of different lengths into Neuro2A cells. The predicted Sox10 responsive regions are shown as filled circles. (*B*) Sox10-dependent induction was recognized between base pair −279 and base pair −328 and between base pair −538 and base pair −858. (*C*) Three Sox10 binding sites, S1 (base pair −287 to base pair −293), S2 (base pair −592 to base pair −600), and S3 (base pair −660 to base pair −666) were identified with mutant reporter constructs (Fig. 7*B*) by cotransfection with Sox10. S1m showed remarkable reduction (44%), S2m showed lower reduction (72%), and S3 showed only modest reduction (83% activity in comparison to nonmutant wild-type construct). Mutation of all three Sox10 binding sites virtually abolished Sox10-dependent promoter activity.

positive control [Sox10 consensus high mobility group type DNA-binding motif (SX)] and S1-, S2-, and S3-specific oligonucleotides (Fig. 4*B*). Furthermore, a supershifted band was recognized with a Sox10 antiserum for the S1 site (Fig. 4*C*). Weak but specific supershifted bands were also recognized for the S2 and S3 sites (results not shown). There was no oligo–protein complex recognized (Fig. 4*C*) with mutated oligos for the S1 site (see Table 1), indicating specificity of the supershift experiment.

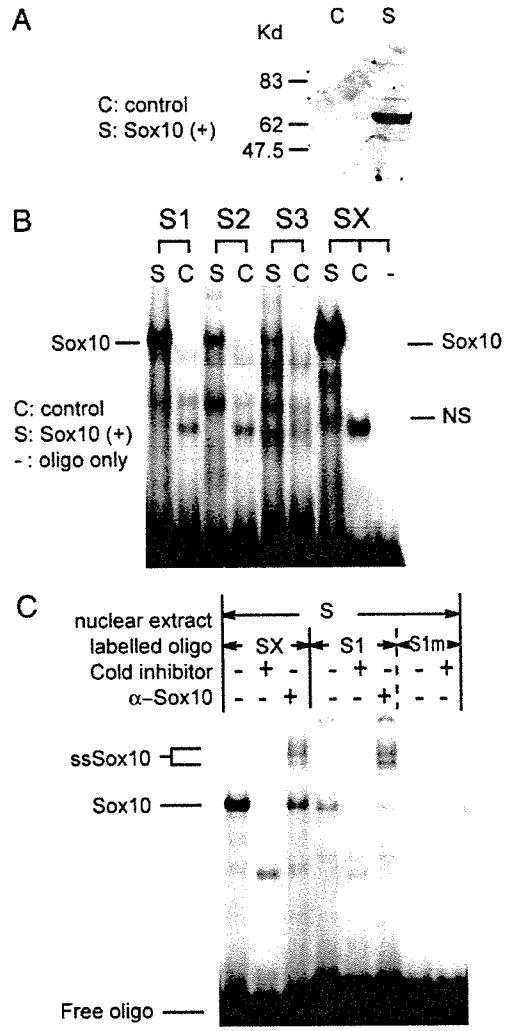

Fig. 4. Sox10 binding to S1, S2, and S3 sites in the *Cntf* promoter. (*A*) Western blot analysis of nuclear extract from COS cells transfected by Sox10 expression vector (S) and pcDNA3 control vector (C). Sox10 immunoreactivity was recognized as a single band at 64 kDa. (*B*) Sox10 binds to S1, S2, and S3 sites. SX is a consensus oligonucleotide for Sox10 (Table 1). S indicates the nuclear extract cotransfected with Sox10 expression vector, and C indicates the nuclear extract cotransfected with pcDNA3 empty vector. NS indicates nonspecific band. (*C*) A supershifted band was recognized with the Sox10 antiserum and oligonucleotide corresponding to the Sox1 site. Weak interaction was also observed for S2 and S3 (unpublished data). No oligo–protein complex recognized with mutated oligo (S1m). ssSox10, supershifted Sox10.

Discussion

Control of myelin gene expression involves concerted actions of several transcription factors (1). Here we show that Cntf expression is also controlled by transcription factors previously identified in the context of Schwann cell differentiation and myelin formation. Among these, Sox10 plays a pivotal role for Cntf up-regulation in early postnatal Schwann cells. After birth, Sox10 expression is found at P1 and strongly increases at P3 in mice. The raise in Sox10 levels is followed by a strong increase of Cntf expression at P7. Moreover, the importance of Sox10 is underlined by our observation that Cntf protein levels are significantly reduced in sciatic nerves of *Sox10+/−* mice, even stronger than levels of P0 protein (data not shown).

Surprisingly, Pax3 appears as a repressor of *Cntf* promoter activity in our cotransfection studies. Pax3 also reduced the positive

regulatory effect of Sox10. Pax3 is indispensable for the differentiation of neural crest derivatives (36). Its expression in peripheral nerves of embryonic mice is high, and expression goes down around birth before Cntf expression is up-regulated. It appears tempting to speculate that Pax3 represses expression of Cntf during embryonic development and that the down-regulation of Pax3 around birth contributes to the massive up-regulation of Cntf production starting in the first postnatal week.

Interestingly, patients with deletion or mutations in the *Sox10* gene reveal defects in the peripheral nervous system known as Hirschsprung disease (37, 38). In such patients, defects of the enteric ganglia and subsequently a lack of coordinated innervation of bowel and gut are prevailing, but peripheral neuropathies are also part of the disease phenotype (39). It is not clear whether the neuropathy can simply be explained as a defect in proper myelination in such patients (40). It is likely that Sox10 controls additional target genes that influence maintenance and function of the peripheral nervous system. Thus, reduced Cntf levels could contribute to this phenotype. Levels of Cntf protein in human peripheral nerves are much lower than in mice (M.S., unpublished observations), and human CNTF is less active than the mouse Cntf protein, even in human target cells (41). Thus, reduced gene expression might be more critical in humans in comparison to mice. In postnatal *Cntf*−/− mice, loss of motoneurons occurs (17), and degenerative alterations in Schwann cell morphology such as disintegration of paranodal networks are detectable at nodes of Ranvier (42). Furthermore, reduced Cntf levels exaggerate the disease phenotype when combined with the *superoxide dismutase 1* (*SOD1*) (19) gene mutation resulting in more severe motoneuron disease. Thus, reduced Cntf expression might also be relevant for the pathophysiology of neuropathies caused by mutations in *Sox10* or other conditions reducing Sox10 levels.

In summary, our data indicate that Sox10 up-regulates *Cntf* gene expression in Schwann cells and other cell types and that Cntf protein levels are reduced in *Sox10* mutant mice. Dysregulation of Cntf expression could contribute to the phenotype of specific neuropathies, in particular those caused by mutations in *Sox10*.

Materials and Methods

Cloning and Sequencing of Murine *Cntf* Promoter. A genomic clone containing a 6.5-kb insert with the complete *Cntf* gene was obtained by screening bacterial artificial chromosome filters (Incyte Genomics, Palo Alta, CA). Digestion of a positive bacterial artificial chromosome with EcoRV, subcloning into pBSII KS+/−, and DNA sequencing revealed that this clone also contained the 4.7-kb 5′ promoter region of *Cntf* including the 3′ region of the *Zfp* gene, which is located upstream of *Cntf*.

Computer Analysis of Putative Binding Sites for Transcription Factors in the Cntf Promoter. Programs provided by the Genetics Computer Group (Madison, WI) and MATINSPECTOR PROFESSIONAL (Genomatix, Munich) (43) were used for sequence analysis of the *Cntf* promoter.

RNA Extraction, 5′ and 3′ RACE (Oligo Cap Methods). Total RNA was isolated from adult mouse sciatic nerve by TRIzol (Invitrogen) according to the manufacturer's protocol. The 5′ and 3′ RACE were performed as described in *Supporting Methods*, which is published as supporting information on the PNAS web site.

Plasmid Constructs, Cell Culture, Transfection, and Luciferase Assays. DNA corresponding to various regions of the *Cntf* promoter was cloned by PCR with appropriate sense and antisense primers (Cz10rev2) (Table 2, which is published as supporting information on the PNAS web site). Cloning of expression and reporter constructs is described in *Supporting Methods*.

NIH 3T3, Cos7, Neuro2A, and IMS32 Schwann cell lines (27) and primary Schwann cells were maintained in Dulbecco–Vogt-modified Eagle's medium with 10% FCS, 50 units/ml penicillin, and 100 μg/ml streptomycin. Transfection was performed as described in *Supporting Methods* and Table 1.

Nuclear Protein Extraction and Western Blotting. Cos7 and Neuro2A cells were transfected with 37.5 μg of expression vectors for Sox10 in 100-mm dishes. In parallel, pcDNA3 vector was transfected as a control. After 24 h, cells were harvested, and nuclear extracts were collected (44). Protein concentration was measured by using a Bradford assay. Nuclear protein extracts (25 μg) were subjected to Western blotting. Anti-Sox10 antibody (45) was used at a 1:3,000 dilution. The Cntf antiserum K10 was used at a 1:5,000 dilution. Recombinant rat Cntf was used as a standard for analysis of Cntf expression levels.

EMSA. Double-stranded 30- or 34-bp oligonucleotides (1 μg) were radiolabeled by extension of overhanging GATC 4-bp ends with Klenow fragment of DNA polymerase in the presence of [α-^{32}P]dCTP. Labeled oligonucleotide and 4 μg of nuclear protein were incubated in 20 μl of reaction mixture. Reaction mixture for Sox10 contained 10 mM Hepes (pH 8.0), 50 mM NaCl, 5 mM $MgCl_2$, 0.1 mM EDTA, 2 mM DTT, 5% glycerol, 10% BSA, and 2 μg of poly[d(I)d(C)] (Sigma). For competition experiments, unlabeled double-stranded oligonucleotides were preincubated in 250-fold excess with the protein for 20 min before labeled oligonucleotides were added. Supershifts were performed by using an antibody to Sox10 as described (45). All samples were electrophoresed on 5% native polyacrylamide gels for 1.5 h at 140 V. Gels were dried after electrophoresis and exposed to X-OMAT film (Kodak) to detect radioactivity.

Western Blot Analysis. Sciatic nerves were dissected from P1, P3, P7, and P42 wild-type and *Sox10*+/− mice (8). Cell lysates from Sox10 RNA interference-transfected IMS32 cells were harvested 24 h after transfection. Protein extracts were prepared and processed for Cntf and Sox10 (46) Western blot analysis. Blots were then stripped and reacted with antibodies against actin (MAB1501R; Chemicon). Signal intensities were measured and normalized against the actin signal (AIDA software package; Raytest, Straubenhardt, Germany). Statistical analysis was performed by using the unpaired two-tailed *t* test (PRISM; GraphPad, San Diego).

We thank Michaela Pfister for technical assistance. This work was supported by the Deutsche Forschungsgemeinschaft (SFB581), grants from the Japan Foundation for Aging and Health (to Y.I.), and the Kanae Foundation for Life & Socio-Medical Science.

1. Wegner, M. (2000) *Glia* **29**, 118–123.
2. Kioussi, C., Gross, M. K. & Gruss, P. (1995) *Neuron* **15**, 553–562.
3. Monuki, E. S., Weinmaster, G., Kuhn, R. & Lemke, G. (1989) *Neuron* **3**, 783–793.
4. Jaegle, M., Mandemakers, W., Broos, L., Zwart, R., Karis, A., Visser, P., Grosveld, F. & Meijer, D. (1996) *Science* **273**, 507–510.
5. Bermingham, J. R., Jr., Scherer, S. S., O'Connell, S., Arroyo, E., Kalla, K. A., Powell, F. L. & Rosenfeld, M. G. (1996) *Genes Dev.* **10**, 1751–1762.
6. Arroyo, E. J., Bermingham, J. R., Jr., Rosenfeld, M. G. & Scherer, S. S. (1998) *J. Neurosci.* **18**, 7891–7902.
7. Kuhlbrodt, K., Schmidt, C., Sock, E., Pingault, V., Bondurand, N., Goossens, M. & Wegner, M. (1998) *J. Biol. Chem.* **273**, 23033–23038.
8. Britsch, S., Goerich, D. E., Riethmacher, D., Peirano, R. I., Rossner, M., Nave, K. A., Birchmeier, C. & Wegner, M. (2001) *Genes Dev.* **15**, 66–78.
9. Stöckli, K. A., Lottspeich, F., Sendtner, M., Masiakowski, P., Carroll, P., Götz, R., Lindholm, D. & Thoenen, H. (1989) *Nature* **342**, 920–923.
10. Stöckli, K. A., Lillien, L. E., Näher-Noe, M., Breitfeld, G., Hughes, R. A., Thoenen, H. & Sendtner, M. (1991) *J. Cell Biol.* **115**, 447–459.
11. Stahl, N. & Yancopoulos, G. D. (1994) *J. Neurobiol.* **25**, 1454–1466.
12. Ip, N. Y. & Yancopoulos, G. D. (1996) *Annu. Rev. Neurosci.* **19**, 491–515.

13. Bonni, A., Sun, Y., Nadal-Vicens, M., Bhatt, A., Frank, D. A., Rozovsky, I., Stahl, N., Yancopoulos, G. D. & Greenberg, M. E. (1997) *Science* **278**, 477–483.
14. Sendtner, M., Kreutzberg, G. W. & Thoenen, H. (1990) *Nature* **345**, 440–441.
15. Sendtner, M., Stöckli, K. A. & Thoenen, H. (1992) *J. Cell Biol.* **118**, 139–148.
16. Sendtner, M., Götz, R., Holtmann, B. & Thoenen, H. (1997) *J. Neurosci.* **17**, 6999–7006.
17. Masu, Y., Wolf, E., Holtmann, B., Sendtner, M., Brem, G. & Thoenen, H. (1993) *Nature* **365**, 27–32.
18. DeChiara, T. M., Vejsada, R., Poueymirou, W. T., Acheson, A., Suri, C., Conover, J. C., Friedman, B., McClain, J., Pan, L., Stahl, N., *et al.* (1995) *Cell* **83**, 313–322.
19. Giess, R., Holtmann, B., Braga, M., Grimm, T., Muller-Myhsok, B., Toyka, K. V. & Sendtner, M. (2002) *Am. J. Hum. Genet.* **70**, 1277–1286.
20. Giess, R., Maurer, M., Linker, R., Gold, R., Warmuth-Metz, M., Toyka, K. V., Sendtner, M. & Rieckmann, P. (2002) *Arch. Neurol. (Chicago)* **59**, 407–409.
21. Linker, R. A., Maurer, M., Gaupp, S., Martini, R., Holtmann, B., Giess, R., Rieckmann, P., Lassmann, H., Toyka, K. V., Sendtner, M., *et al.* (2002) *Nat. Med.* **8**, 620–624.
22. Sendtner, M., Schmalbruch, H., Stöckli, K. A., Carroll, P., Kreutzberg, G. W. & Thoenen, H. (1992) *Nature* **358**, 502–504.
23. Mitsumoto, H., Ikeda, K., Holmlund, T., Greene, T., Cedarbaum, J. M., Wong, V. & Lindsay, R. M. (1994) *Ann. Neurol.* **36**, 142–148.
24. Dobrea, G. M., Unnerstall, J. R. & Rao, M. S. (1992) *Dev. Brain Res.* **66**, 209–219.
25. Herbarth, B., Pingault, V., Bondurand, N., Kuhlbrodt, K., Hermans-Borgmeyer, I., Puliti, A., Lemort, N., Goossens, M. & Wegner, M. (1998) *Proc. Natl. Acad. Sci. USA* **95**, 5161–5165.
26. Southard-Smith, E. M., Kos, L. & Pavan, W. J. (1998) *Nat. Genet.* **18**, 60–64.
27. Watabe, K., Fukuda, T., Tanaka, J., Honda, H., Toyohara, K. & Sakai, O. (1995) *J. Neurosci. Res.* **41**, 279–290.
28. Saotome, Y., Winter, C. G. & Hirsh, D. (1995) *Gene* **152**, 233–238.
29. Carroll, P., Sendtner, M., Meyer, M. & Thoenen, H. (1993) *Glia* **9**, 176–187.
30. Pritchard, C., Grosveld, G. & Hollenbach, A. D. (2003) *Gene* **305**, 61–69.
31. Faus, I., Hsu, H. J. & Fuchs, E. (1994) *Mol. Cell. Biol.* **14**, 3263–3275.
32. Schlierf, B., Ludwig, A., Klenovsek, K. & Wegner, M. (2002) *Nucleic Acids Res.* **30**, 5509–5516.
33. Peirano, R. I., Goerich, D. E., Riethmacher, D. & Wegner, M. (2000) *Mol. Cell. Biol.* **20**, 3198–3209.
34. Watabe, K., Sakamoto, T., Kawazoe, Y., Michikawa, M., Miyamoto, K., Yamamura, T., Saya, H. & Araki, N. (2003) *Neuropathology* **23**, 68–78.
35. Wegner, M. (1999) *Nucleic Acids Res.* **27**, 1409–1420.
36. Goulding, M. D., Chalepakis, G., Deutsch, U., Erselius, J. R. & Gruss, P. (1991) *EMBO J.* **10**, 1135–1147.
37. Tassabehji, M., Read, A. P., Newton, V. E., Harris, R., Balling, R., Gruss, P. & Strachan, T. (1992) *Nature* **355**, 635–636.
38. Hoth, C. F., Milunsky, A., Lipsky, N., Sheffer, R., Clarren, S. K. & Baldwin, C. T. (1993) *Am. J. Hum. Genet.* **52**, 455–462.
39. Cheng, W., Au, D. K., Knowles, C. H., Anand, P. & Tam, P. K. (2001) *J. Pediatr. Surg.* **36**, 296–300.
40. Inoue, K., Shilo, K., Boerkoel, C. F., Crowe, C., Sawady, J., Lupski, J. R. & Agamanolis, D. P. (2002) *Ann. Neurol.* **52**, 836–842.
41. Wong, V., Pearsall, D., Arriaga, R., Ip, N. Y., Stahl, N. & Lindsay, R. M. (1995) *J. Biol. Chem.* **270**, 313–318.
42. Gatzinsky, K. P., Holtmann, B., Daraie, B., Berthold, C. H. & Sendtner, M. (2003) *Glia* **42**, 340–349.
43. Quandt, K., Frech, K., Karas, H., Wingender, E. & Werner, T. (1995) *Nucleic Acids Res.* **23**, 4878–4884.
44. Sock, E., Leger, H., Kuhlbrodt, K., Schreiber, J., Enderich, J., Richter-Landsberg, C. & Wegner, M. (1997) *J. Neurochem.* **68**, 1911–1919.
45. Kuhlbrodt, K., Herbarth, B., Sock, E., Enderich, J., Hermans-Borgmeyer, I. & Wegner, M. (1998) *J. Biol. Chem.* **273**, 16050–16057.
46. Stolt, C. C., Lommes, P., Sock, E., Chaboissier, M. C., Schedl, A. & Wegner, M. (2003) *Genes Dev.* **17**, 1677–1689.

Journal of Neurochemistry, 2006 doi:10.1111/j.1471-4159.2006.03885.x

High glucose-induced activation of the polyol pathway and changes of gene expression profiles in immortalized adult mouse Schwann cells IMS32

Kazunori Sango,* Takeshi Suzuki,† Hiroko Yanagisawa,* Shizuka Takaku,* Hiroko Hirooka,† Miyuki Tamura† and Kazuhiko Watabe‡

**Department of Developmental Morphology, Tokyo Metropolitan Institute for Neuroscience, Fuchu, Tokyo, Japan*

†Pharmaceutical Research Laboratories, Sanwa Kagaku Kenkyusho Co. Ltd, Inabe, Japan

‡Department of Molecular Neuropathology, Tokyo Metropolitan Institute for Neuroscience, Fuchu, Tokyo, Japan

Abstract

We investigated the polyol pathway activity and the gene expression profiles in immortalized adult mouse Schwann cells (IMS32) under normal (5.6 mM) and high (30 and 56 mM) glucose conditions for 7–14 days in culture. Messenger RNA and the protein expression of aldose reductase (AR) and the intracellular sorbitol and fructose contents were up-regulated in IMS32 under high glucose conditions compared with normal glucose conditions. By employing DNA microarray and subsequent RT–PCR/northern blot analyses, we observed significant up-regulation of the mRNA expressions for serum amyloid A3 (SAA3), angiopoietin-like 4 (ANGPTL4) and ecotropic viral integration site 3 (Evi3), and the down-regulation of aldehyde reductase (AKR1A4) mRNA expression in the cells under high glucose (30 mM) conditions. The application of an AR inhibitor, SNK-860, to the high glucose medium ameliorated the increased sorbitol and fructose contents and the reduced AKR1A4 mRNA expression, while it had no effect on mRNA expressions for SAA3, ANGPTL4 or Evi3. Considering that the exposure to the high glucose (≥ 30 mM) conditions mimicking hyperglycaemia *in vivo* accelerated the polyol pathway in IMS32, but not in other previously reported Schwann cells, the culture system of IMS32 under those conditions may provide novel findings about the polyol pathway-related abnormalities in diabetic neuropathy.

Keywords: aldehyde reductase, diabetic neuropathy, DNA microarray, immortalized Schwann cells, polyol pathway.

J. Neurochem. (2006) 10.1111/j.1471-4159.2006.03885.x

Peripheral neuropathy is one of the most common complications of diabetes mellitus, as are retinopathy and nephropathy. Both metabolic alterations in the cellular components (mainly neurons and Schwann cells) and microvascular abnormalities are thought to play major roles in the development of diabetic neuropathy (Mizisin and Powell 2003), although the detailed pathogenesis remains unclear. Schwann cells are responsible for the action potential velocity through the insulation of axons, the maintenance of axonal caliber, effective nerve regeneration after axonal injury and other neural functions in the peripheral nervous system (Eckersley 2002). Therefore, Schwann cell abnormalities as a result of hyperglycaemia can be a cause of nerve dysfunction, such as reduced nerve conduction velocity, axonal atrophy and impaired axonal regeneration (Dyck and Giannini 1996; Song *et al.* 2003; Yasuda *et al.* 2003). The role of Schwann cells in diabetic neuropathy is often discussed in relation to polyol pathway hyperactivity (Eckersley 2002; Mizisin and Powell 2003). Aldose reductase (AR; EC 1.1.1.21) is the first enzyme in the polyol pathway and converts glucose to sorbitol using NADPH as a

Received September 27, 2005; revised manuscript received January 8, 2006; accepted March 5, 2006.

Address correspondence and reprint requests to Kazunori Sango, Department of Developmental Morphology, Tokyo Metropolitan Institute for Neuroscience, 2–6 Musashidai, Fuchu, Tokyo 183–8526, Japan. E-mail: kazsango@tmin.ac.jp

Abbreviations used: ADH, alcohol dehydrogenase; AKR, aldo–keto reductase; ALDH, aldehyde dehydrogenase; ANGPTL4, angiopoietin-like 4; AR, aldose reductase; DRG, dorsal root ganglia; Evi3, ecotropic viral integration site 3; LPL, lipoprotein lipase; NO, nitric oxide; PPAR, peroxisome proliferator-activated receptor; $p75^{NTR}$, p75 low-affinity nerve growth factor receptor; SAA3, serum amyloid A3; SDH, sorbitol dehydrogenase; STZ, streptozotocin.

cofactor. Because AR is localized to Schwann cells in the peripheral nerves (Kern and Engerman 1982), it has been proposed that the activation of AR in Schwann cells under hyperglycaemic conditions affects nerve functions through various mechanisms: (i) sorbitol accumulation leads to osmotic stress and the depletion of myo-inositol and taurine (Tomlinson 1999; Pop-Busui *et al.* 2001); (ii) the increase in AR activity competes with nitric oxide (NO) synthase or glutathione reductase for NADPH. The inhibition of NO synthase and the subsequent decrease in NO in the nervous tissue causes diminished nerve flow, whereas the depletion of reduced glutathione by glutathione reductase inhibition results in the excessive production of free radicals (Low *et al.* 1999); (iii) sorbitol is converted to fructose by sorbitol dehydrogenase (SDH, EC 1.1.1.14), the second enzyme in the polyol pathway. Fructose and its metabolites, such as fructose-6-phosphate and triose-phosphate, can be triggers of non-enzymatic glycation of cellular proteins and lipids (Takagi *et al.* 1995).

Culture systems of Schwann cells appear to be useful for investigating the role of polyol pathway hyperactivity in the pathogenesis of diabetic neuropathy. Thus far, an established Schwann cell line, JS1 (Mizisin *et al.* 1996), and primary cultured adult rat Schwann cells (Suzuki *et al.* 1999; Maekawa *et al.* 2001) have been introduced to study polyol metabolism, but these cells did not display intracellular sorbitol accumulation or enhanced AR expression/enzyme activity under high glucose (25–30 mM) conditions unless hyperosmotic stress (greater than 100 mM) was applied. The reasons for this remain unknown. We have established a spontaneously immortalized Schwann cell line, IMS32, from long-term cultures of adult mouse dorsal root ganglia (DRG) and peripheral nerves (Watabe *et al.* 1995). Because IMS32 possesses some biological properties of mature Schwann cells and high proliferation activity (Watabe *et al.* 1995; Sango *et al.* 2004), this cell line is suitable for functional and biochemical studies of the peripheral nervous system. Kato and colleagues reported that the proliferation activity of IMS32 was decreased by exposure to high glucose (20–40 mM) conditions (Kato *et al.* 2003; Nakamura *et al.* 2003), but the polyol metabolism in the cells has not yet been characterized. If the polyol pathway is activated in IMS32 in response to the high glucose concentrations mimicking hyperglycaemia *in vivo*, this cell line would be a valuable tool for the study of diabetic neuropathy. In the present study, we investigated the mRNA expression of AR and SDH, the protein expression of AR and the intracellular contents of sorbitol and fructose in IMS32 under high glucose (30 and 56 mM) and hyperosmotic (50 mM of sodium chloride) conditions. We also employed DNA microarray and subsequent RT–PCR/northern blot analyses to see the high glucose (30 mM)-induced alterations in the gene expression profiles, especially in association with the polyol pathway activity.

Materials and methods

Preparation of the plasmid-containing mouse cDNAs for AR and SDH

The plasmids containing mouse AR and SDH cDNA fragments were created by PCR cloning, as described previously (Sango *et al.* 2004). Briefly, total RNA was isolated from IMS32 using Sepazol reagent (Nacalai Tesque, Kyoto, Japan), and was reverse transcribed with M-MLV reverse transcriptase (Invitrogen, Groningen, the Netherlands) and pd$(N)_6$ random primer (Amersham Pharmacia Biotech, Piscataway, NJ, USA). The synthesized cDNA was used as a template for the PCR reaction. The PCR primers were designed to amplify the 896 bp of mouse AR [aldo–keto reductase 1B3 (AKR1B3)] gene (sense primer 5′-ATGGCCAGCCATCTGGA-ACTC-3′ and antisense primer 5′-CACACCCTCCAGTTCCTGTT-3′) (GenBank accession no. NM_009658) and the 1074 bp of mouse SDH gene (sense primer 5′-ATGGCAGCTCCAGCT-AAGGGC-3′ and antisense primer 5′-CTAGGGGTTTTGGT-CATTGGG-3′) (GenBank accession no. NM_146126). The PCR products were subcloned into pGEM-T Easy Vector (Promega, Madison, WI, USA) according to the manufacturer's instructions, and the resulting plasmid DNA was sequenced (Promega/Bex Co. Ltd, Tokyo, Japan).

Cell culture

Immortalized adult mouse Schwann cells (IMS32) were seeded on 75-cm^2 flasks (Nalge Nunc International, Naperville, IL, USA) at a density of 5×10^4/cm^2 and cultured in Dulbecco's modified Eagle's medium (DMEM; Sigma, St Louis, MO, USA) supplemented with 10% fetal calf serum (FCS; Invitrogen). The medium contained 5.6 mM glucose. When the cells reached approximately 80–85% confluency, they were maintained in DMEM supplemented with 1% FCS and containing 5.6 mM glucose (Glc-5.6), 30 mM glucose (Glc-30), 56 mM glucose (Glc-56) or 5.6 mM glucose and 50 mM sodium chloride (NaCl-50). The media containing a low concentration (1%) of serum slowed the proliferation of IMS32, and made it possible to keep the cultures in the same culture flasks for up to 14 days without detachment and the re-seeding of cells. Seven days after incubation under each experimental condition, the cells were rinsed with phosphate-buffered saline (PBS, Sigma) and detached from the flasks by cell scrapers (Sumitomo Bakelite Co. Ltd, Tokyo, Japan). These cells were suspended in 2 mL of sterile water and collected in sterile tubes for use in northern blotting or western blotting.

Northern blotting

The cDNA fragments of AR and SDH (10 ng/mL) were prepared from the plasmids, and labelled with alkaline phosphatase [AlkPhos Direct (Amersham Pharmacia Biotech)] according to the manufacturer's instructions. Total RNA was isolated from the cells using Sepazol reagent, and the concentration of RNA was determined with a spectrophotometer (Gene Quant Pro; Amersham Pharmacia Biotech). Twenty-five micrograms of total RNA was electrophoresed in 1% agarose-formaldehyde gel and transferred to Hybond N+ membrane (Amersham Pharamacia Biotech). We prepared two membranes with the same RNA samples; one was stained with methylene blue (Waldeck-Gmbh and Co KG, Münster, Germany) and the other was hybridized overnight at 50°C with the labelled probes. The CDP-Star™ chemiluminescent detection reagent and

Hyperfilm ECL (Amersham Pharamacia Biotech) were used for visualization of the positive signals (Sango *et al.* 2004). The band intensity was quantified with Edas 290 1D Image Analysis software (Eastman Kodak, New York, NY, USA; Sango *et al.* 2002), and the abundance of mRNA was expressed as a 'relative expression' (the intensity in each experimental group relative to that in Glc-5.6). 28S ribosomal RNA stained with methylene blue on the duplicate membranes was used for standardization.

Western blotting

Cells were homogenized with a cell sonicator (Tomy Seiko Co. Ltd, Tokyo, Japan), and the concentration of protein was determined by using a DC Protein Assay (Bio-Rad Laboratories, Hercules, CA, USA) according to the manufacturer's instructions. Twenty micrograms of protein were electrophoresed on 14–16% gradient sodium dodecyl sulfate – polyacrylamide gel electrophoresis (Daiichi Pure Chemical Co. Ltd, Tokyo, Japan) under non-reducing conditions and transferred to nitrocellulose paper (Bio-Rad Laboratories). The blotted paper was then blocked with 5% skimmed milk and incubated for 1 h at room temperature (25°C) with goat polyclonal anti-AR antibody [ALR2 (P-20), 1 : 2000; Santa Cruz Biotechnology, Santa Cruz, CA, USA] or mouse monoclonal anti-β-actin antibody (1 : 1000; Sigma), followed by incubations with biotinylated anti-goat IgG or anti-mouse IgG (1 : 1000; Vector Laboratories, Burlingame, CA, USA), and streptoavidin–alkaline phosphatase (1 : 1000; Promega). Reactions were visualized by colour development using Western blue® stabilized substrate for alkaline phosphatase (Promega).

Immunocytochemistry

IMS32 were seeded on wells of 8-well chamber slides (Nalge Nunc) or Aclar fluorocarbon coverslips (Nissin EM Co. Ltd, Tokyo, Japan; 9 mm in diameter) at a density of $1–2 \times 10^4/cm^2$, and kept in Glc-5.6, Glc-30, Glc-56 or NaCl-50 for 7 days. Then, the cells were fixed with 4% paraformaldehyde for 15 min at 4°C with the following antibodies (diluted with 20 mM PBS containing 0.5% skimmed milk): (i) goat anti-AR polyclonal antibody (1 : 3000); (ii) rabbit anti-S100 polyclonal antibody (1 : 3000; Dako, Carpinteria, CA, USA); (iii) rabbit anti-p75 low-affinity nerve growth factor receptor ($p75^{NTR}$) polyclonal antibody (1 : 1000; Promega).

After rinsing with PBS, the cells were incubated for 1 h at 37°C with peroxidase-conjugated anti-goat IgG (for AR) or anti-rabbit IgG (for S100 and $p75^{NTR}$) antibody (1 : 100, Vector Laboratories). The immunoreaction was visualized under a light microscope using 0.01% diaminobenzidine tetrahydro-chloride (DAB; Wako Co., Tokyo, Japan) and 0.01% hydrogen peroxide in 50 mM Tris buffer (pH 7.4) at room temperature for 15 min (Sango *et al.* 2004).

Measurement of the intracellular contents of sorbitol and fructose

IMS32 were seeded on wells of 6-well plates (Corning Inc., Corning, NY, USA) at a density of $5 \times 10^4/cm^2$, and kept in Glc-5.6 or Glc-30 for 14 days. A subset of Glc-30 was treated with 1 μM of an AR inhibitor, SNK-860 (Sanwa Kagaku Kenkyusho Co. Ltd, Inabe, Japan) for 7 days (from 7 to 14 days in culture). This culture condition was termed Glc-30/SNK. Cells under each experimental condition were rinsed in ice-cold PBS and homogenized in 2 mL of cold water with a cell sonicator. Protein concentrations were determined by using a DC Protein Assay (Bio-Rad Laboratories) according to the manufacturers' instructions. The polyol level in each lyophilized sample was determined by liquid chromatography with tandem mass spectrometry, according to the method of Guerrant and Moss (1984). The value of polyol was expressed as nmol/mg protein.

DNA microarray analysis

IMS32 cells were kept in Glc-5.6 or Glc-30 for 14 days in 175-cm^2 flasks (Nalge Nunc), and the total RNA was isolated from the cells using an RNeasy mini kit (Qiagen, Tokyo, Japan). The DNA microarray analysis was performed with these samples (Custom Technology Service by Kurabo Industries Ltd, Osaka, Japan). Briefly, total RNA was reverse transcribed to cDNA with T7 oligo d(T) primer (Amersham Pharmacia Biotech). The cDNA synthesis product was used in an *in vitro* transcription reaction containing T7 RNA polymerase and biotinylated uridine triphosphate. Then, the labelled cRNA products were fragmented, loaded onto CodeLink™ Uniset Mouse 20K Bioarray (Amersham Pharmacia Biotech) and hybridized according to the manufacturer's protocol. Streptavidin-Cy5 (Amersham Pharmacia Biotech) was used as the fluorescent conjugate to detect hybridized target sequences. Raw intensity data from the Codelink Bioarray were analyzed in Microsoft Excel (Microsoft, Redmond, WA, USA) and gene expression levels were expressed as relative intensities (intensity data in Glc-30 compared with those in Glc-5.6). Only the fold changes of relative intensities >2.0 and <0.5 were considered to be significant up-regulations and down-regulations, respectively.

Confirmation of high glucose-responsive gene expression by RT–PCR and northern blot analyses

Total RNA was isolated from the cells kept in Glc-5.6, Glc-30 or Glc-30/SNK for 14 days in 75-cm^2 flasks by using Sepazol reagent. Semi-quantitative RT–PCR analysis was carried out as described previously (Sango *et al.* 2002). Briefly, first-strand cDNA was synthesized from 4 μg of total RNA and PCR amplification was performed in a reaction volume of 25 μL containing 2 μL of diluted cDNA, 0.625 U of AmpliTaqGold™ DNA polymerase (Applied Biosystems, Foster City, CA, USA), each dNTP at 0.2 mM, 50 mM KCl, 10 mM Tris-HCl (pH 8.3), 1.5 mM $MgCl_2$ and sense and antisense primers each at 0.5 μM. Oligonucleotide sense and antisense primers for the PCR were as follows: serum amyloid A3 (SAA3; GenBank accession no. NM_011315), 5′-ATGAAGCCTTCCATTGCCA-3′ and 5′-TATCTTTTAGGCAGGCAGGCCAGCA-3′ (a 365-bp product); angiopoietin-like 4 (ANGPTL4; GenBank accession no. NM_020581), 5′-AGGGGCCCAAGGGAAAAGAT-3′ and 5′-TAGCCTCCATGGGCTGGAT-3′ (a 978-bp product); ecotropic viral integration site 3 (Evi3; GenBank accession no. NM_145492), 5′-TGGGGAGGCAGTAGACTG-3′ and 5′-CTCCATCCTGGAGCCAGA-3′ (a 640-bp product); β-actin (the internal standard; GenBank accession no. NM_007393), 5′-AGAAGCTGTGCTATGTTGCC-3′ and 5′-ATCCACACAGAGTACTTGCG-3′ (a 382-bp product).

All PCR reactions were carried out under conditions in which the amplification was linear by using the appropriate number of cycles. The PCR products were resolved by electrophoresis in a 2% agarose gel at 100 V for 30 min. The intensity of the PCR fragments visualized by ethidium bromide staining were quantified with

Edas 290, and the abundance of the respective mRNAs was expressed as the intensity of each cDNA fragment/intensity of the β-actin cDNA fragment.

For northern blot analysis, the plasmid-containing mouse aldehyde reductase (AKR1A4; GenBank accession no. NM_021473) cDNA fragment was created by PCR cloning with the following primers: 5′-TCCAGTGTCCTCCTGCACA-3′ and 5′-TCAGTATGGGTCATTAAAGGG-3′ (a 969-bp product).

mRNA expression of SAA3, ANGPTL4, Evi3 and AKR1A4 in the peripheral nerves of adult mice

Three-month-old female ICR mice were anaesthetized by ether and killed, in accordance with the Guideline for the Care and Use of Animals (Tokyo Metropolitan Institute for Neuroscience). Thirty dorsal root ganglia (from the thoracic to sacral levels) with associated spinal nerve bundles were dissected from each mouse, and total RNA was isolated from the dissected tissue as previously described (Sango *et al.* 2002). The cDNA synthesis and subsequent RT–PCR analysis was carried out as described above, using the PCR primers for SAA3, ANGPTL4, Evi3 and AKR1A4.

Statistical analysis

For statistical comparison, post-hoc tests were performed using Bonferroni/Dunn post-hoc analyses. p-values of < 0.05 were considered significant.

Results

IMS32 exhibited Schwann cell phenotypes under normal and high glucose conditions

IMS32 cells showed distinct Schwann cell phenotypes, such as the spindle-shaped morphology (Figs 1a–c) and the expression of Schwann cell markers such as S100 (Figs 1d–f) and $p75^{NTR}$ (not shown) under normal (Glc-5.6; Figs 1a and d) and high glucose conditions (Glc-30 and Glc-56; Figs 1b and e, and Figs 1c and f, respectively). We observed no significant difference in the morphological appearances of living cells or immunoreactivity to S100/$p75^{NTR}$ between Glc-5.6 and Glc-30 or Glc-56. The application of SNK-860 to the high glucose conditions failed to alter these phenotypes of IMS32 (not shown).

Up-regulated AR and SDH mRNA expressions in IMS32 under the high glucose and hyperosmotic conditions

By northern blot analysis with alkaline–phosphatase-labelled cDNA probes, mRNA for AR and SDH were detected as single bands corresponding to the molecular weight of around 1.4 and 2.4 kb molecular size, respectively (Fig. 2a, upper). These results were consistent with those in the previous studies (Gui *et al.* 1995; Lee *et al.* 1995). The blot showed more intense signals for AR mRNA in Glc-30, Glc-56 and NaCl-50 than those in Glc-5.6, and for SDH mRNA in Glc-56 and NaCl-50 than those in Glc-5.6. Methylene blue-stained images of the duplicate membrane (Fig. 2a, lower) showed that a relatively equal amount of RNA was loaded. The average values of the relative expression of AR mRNA were 1 in Glc-5.6, 1.88 in Glc-30, 2.41 in Glc-56 and 2.78 in NaCl-50, respectively (Fig. 2b); AR mRNA expression was up-regulated under the high glucose (Glc-30 and Glc-56) and hyperosmotic (NaCl-50) conditions, although the difference in the values between Glc-30 and Glc-5.6 was not statistically significant. The average values of relative expression of SDH mRNA were 1 in Glc-5.6, 1.19 in Glc-30,

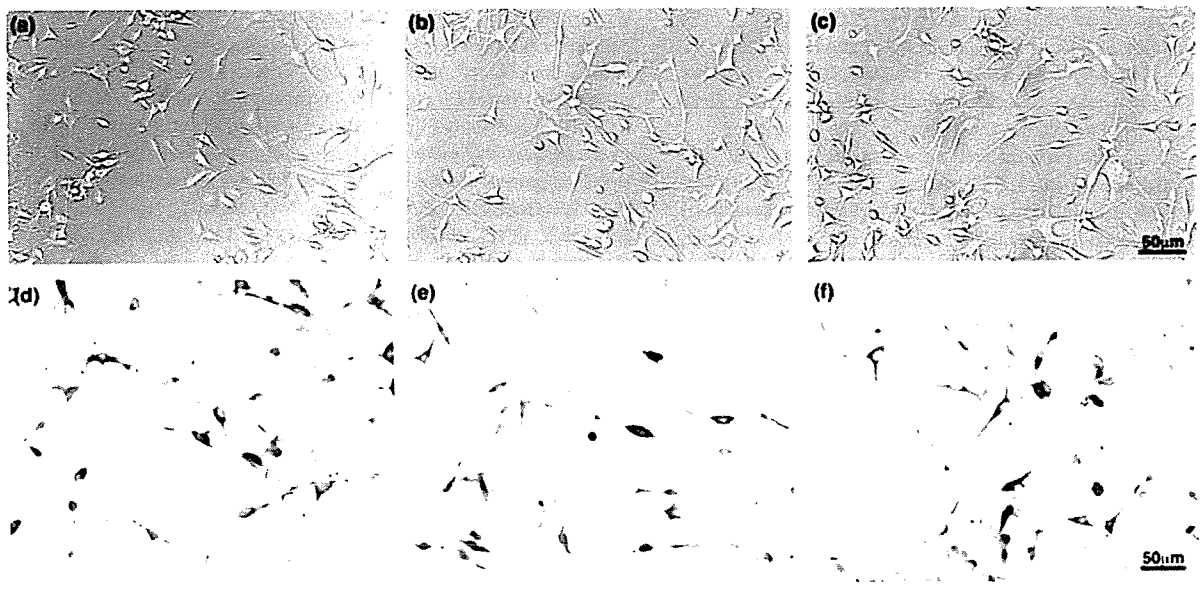

Fig. 1 IMS32 showed distinct Schwann cell phenotypes such as spindle-shaped morphology (a–c) and immunoreactivity to S100 protein (d–f) under normal [Glc-5.6 (a, d)] and high [Glc-30 (b, e) and Glc-56 (c, f)] glucose conditions.

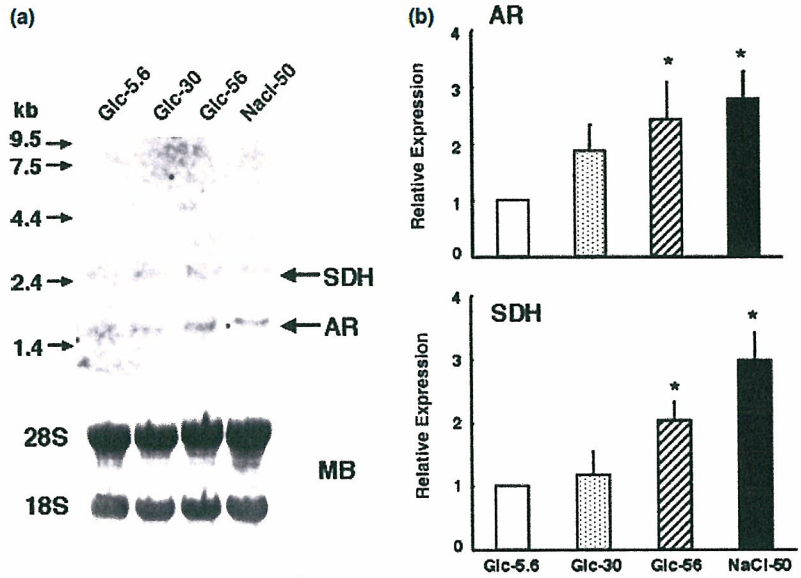

Fig. 2 Relative mRNA expressions of AR and SDH in IMS32 determined by northern blot analysis. (a) The picture of the blot hybridized with alkaline–phosphatase-labelled cDNA probes (upper panel). Marker molecular masses for calibration are indicated on the left. mRNA for AR and SDH were detected as single bands corresponding to the molecular weight of around 1.4 and 2.4 kb, respectively. The blot showed more intense signals for AR mRNA in Glc-30, Glc-56 and NaCl-50 than that in Glc-5.6, and more intense signals for SDH mRNA in Glc-56 and NaCl-50 than that in Glc-5.6. A methylene blue-stained image of the duplicate membrane (lower panel) showed that relatively equal amounts of RNA were loaded. (b) The mRNA expressions of AR (upper panel) and SDH (lower panel) in Glc-30, Glc-56 and NaCl-50 relative to those in Glc-5.6. Values represent the mean + SEM of four experiments. $^*p < 0.05$ (by Bonferroni Dunn post-hoc analysis) as compared with Glc-5.6.

2.03 in Glc-56 and 2.99 in NaCl-50; SDH mRNA expression was significantly up-regulated under the high glucose (Glc-56) and hyperosmotic (NaCl-50) conditions.

Up-regulated AR protein expression under high glucose and hyperosmotic conditions

By western blot analysis with a polyclonal anti-AR antibody, the expression band of AR was identified as the level of around 36 kDa in molecular size (Fig. 3a, upper). The blot showed more intense signals for AR protein in Glc-30, Glc-56 and NaCl-50 than those in Glc-5.6. There was no significant difference in the signal intensity to β-actin between normal and high glucose/hyperosmotic conditions (Fig. 3a, lower). The average values of relative expression were 1 in Glc-5.6, 1.79 in Glc-30, 2.15 in Glc-56 and 1.95 in NaCl-50, respectively; AR protein expression was up-regulated under the high glucose (Glc-30 and Glc-56) and hyperosmotic (NaCl-50) conditions, although the difference in the values between Glc-30 and Glc-5.6 was not statistically significant. Immunocytochemical analysis revealed the localization of AR protein in the cytoplasm of IMS32. The immunoreactivity for AR was markedly enhanced in Glc-30 (Fig. 4b) compared with Glc-5.6 (Fig. 4a), whereas we saw no significant difference in the immunoreactivity for S100 between the two culture conditions (Fig. 1).

Intracellular polyol levels under normal and high glucose conditions

The intracellular contents of sorbitol and fructose were significantly higher in Glc-30 (17.9 ± 1.7 and 77.7 ± 6.7 nmol/mg) than those in Glc-5.6 (1 ± 0.2 and 13.6 ± 3.4 nmol/mg; Fig. 5a). The polyol levels in the cells under Glc-56 were extremely high and beyond the range of measurement. The application of an AR inhibitor, SNK-860, to the high glucose (Glc-30) condition for 7 days significantly reduced the polyol contents to levels close to those under normal glucose (Glc-5.6) conditions (i.e. sorbitol 17.9 ± 1.7 nmol/mg in Glc-30 vs. 3.4 ± 0.4 nmol/mg in Glc-30/SNK and fructose 77.7 ± 6.7 nmol/mg in Glc-30 vs. 29.2 ± 4.8 nmol/mg in Glc-30/SNK). The western blot analysis performed in parallel with the measurement of the polyols revealed that the level of AR protein in Glc-30 was not reduced by treatment with SNK-860 (not shown).

Gene expression profiles in IMS32 under normal and high glucose conditions

Among nearly 20 000 mouse genes, we identified 28 genes with altered expression in the high glucose (Glc-30) conditions; 10 genes were expressed at a 2.0-fold or greater level, while 18 genes were down-regulated by 2.0-fold or more (Table 1). The relative expression of AR mRNA was 1.2

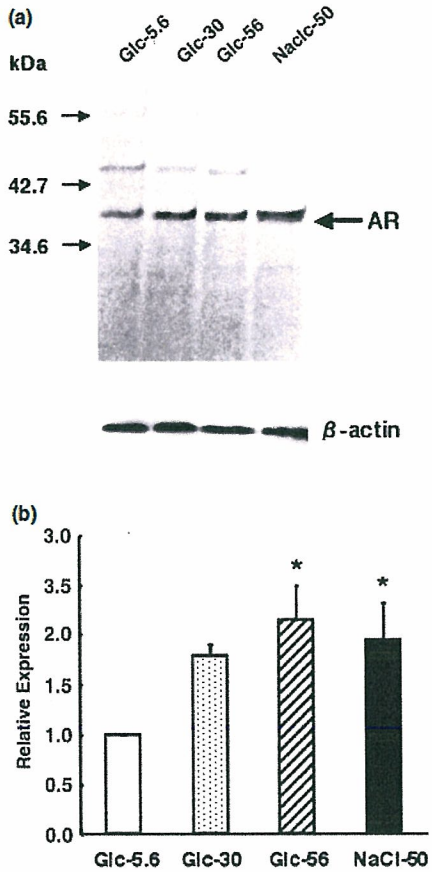

Fig. 3 Relative protein expression of AR in IMS32 determined by western blot analysis. (a) The picture of the blot incubated with a polyclonal anti-AR antibody (upper panel). Marker molecular masses for calibration are indicated on the left. The expression band of AR was identified as the level a molecular size of around 36 kDa. The blot showed more intense signals for AR protein in Glc-30, Glc-56 and NaCl-50 than that in Glc-5.6. The blot incubated with a monoclonal anti-β-actin antibody (lower panel) showed that there was no significant difference in the signal intensity among each experimental group. (b) The protein expression of AR in Glc-30, Glc-56 and NaCl-50 relative to that in Glc-5.6. Values represent the mean + SEM of three experiments. $^*p < 0.05$ as compared with Glc-5.6.

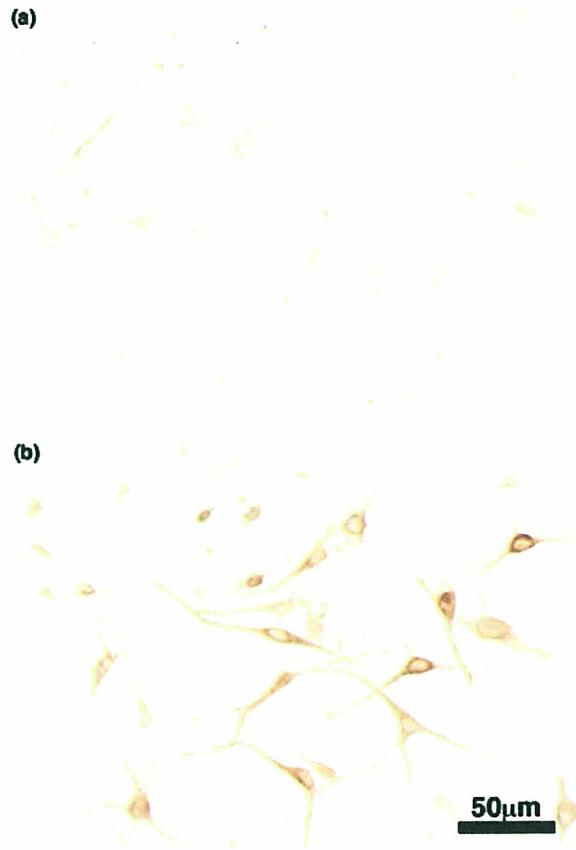

Fig. 4 Immunocytochemical localization of AR protein in the cytoplasm of IMS32. The photomicrographs showed more intense immunoreactivity for AR in Glc-30 (b) than that in Glc-5.6 (a).

(< 2-fold), and therefore AR was not included in the up-regulated genes in the table. To confirm the microarray results, we measured the relative expression of these genes in the cells under Glc-5.6, Glc-30 and Glc-30/SNK by RT–PCR or northern blot analysis. Thus far, RT–PCR analysis resulted in the significant up-regulation of three genes in Glc-30 compared with Glc-5.6 – SAA3, ANGPTL4 and Evi3 (Fig. 6). Northern blot analysis revealed the down-regulation of mRNA expression for aldehyde reductase (EC 1.1.1.2, aka AKR1A4; Fig. 7). Treatment with SNK-860 had no effects on the mRNA expressions for SAA3, ANGPTL4 or Evi3, but restored the diminished mRNA expression for AKR1A4 to a level equivalent to Glc-5.6 (Figs 6 and 7). These four genes were expressed in the DRG and spinal nerves of adult normal mice, as well as in IMS32 cells (Fig. 8).

Discussion

Phenotypic and biochemical features of the Schwann cell line IMS32

IMS32 cells showed distinct Schwann cell phenotypes, such as spindle-shaped morphology and intense immunoreactivity for S100 (Fig. 1), $p75^{NTR}$, laminin and several Schwann cell-specific transcription factors and neurotrophic factors (Watabe *et al.* 1995, 2003). Similar to primary and long-term cultured Schwann cells, IMS32 cells exhibit mitogenic responses to several growth factors [e.g. platelet-derived growth factor BB homodimer (PGDF-BB), acidic and basic fibroblast growth factor (aFGF, bFGF), transforming growth factor (TGF)-β1, 2]. In contrast, IMS32 cells are different

